NASA TECHNICAL NOTE

NASA TN D-7099

NASA TN D-7099

EFFECT OF WING DESIGN ON THE LONGITUDINAL AERODYNAMIC CHARACTERISTICS OF A WING-BODY MODEL AT SUBSONIC SPEEDS

by William P. Henderson and Jarrett K. Huffman

Langley Research Center
Hampton, Va. 23365

NATIONAL AERONAUTICS AND SPACE ADMINISTRATION • WASHINGTON, D. C. • DECEMBER 1972

1. Report No.	2. Government Accession No.	3. Recipient's Catalog No.
NASA TN D-7099		

4. Title and Subtitle	5. Report Date
EFFECT OF WING DESIGN ON THE LONGITUDINAL AERODYNAMIC CHARACTERISTICS OF A WING-BODY MODEL AT SUBSONIC SPEEDS	December 1972
	6. Performing Organization Code

7. Author(s)	8. Performing Organization Report No.
William P. Henderson and Jarrett K. Huffman	L-8562
	10. Work Unit No. 760-67-01-01
9. Performing Organization Name and Address	11. Contract or Grant No.
NASA Langley Research Center Hampton, Va. 23365	
	13. Type of Report and Period Covered
12. Sponsoring Agency Name and Address	Technical Note
National Aeronautics and Space Administration Washington, D.C. 20546	14. Sponsoring Agency Code

15. Supplementary Notes

16. Abstract

An investigation has been conducted to determine the effects of wing camber and twist on the longitudinal aerodynamic characteristics of a wing-body configuration. Three wings were used, each having the same planform (aspect ratio of 2.5 and leading-edge sweep angle of 44^{o}) but differing in amounts of camber and twist (wing design lift coefficient). The wing design lift coefficients were 0, 0.35, and 0.70. The investigation was conducted over a Mach number range from 0.20 to 0.70 at angles of attack up to about 22^{o}. The effect of wing strakes on the aerodynamic characteristics of the cambered wings was also studied. A comparison of the experimentally determined aerodynamic characteristics with theoretical estimates is also included.

17. Key Words (Suggested by Author(s))	18. Distribution Statement
Cambered wings Longitudinal aerodynamic characteristics Subsonic speeds	Unclassified – Unlimited

19. Security Classif. (of this report)	20. Security Classif. (of this page)	21. No. of Pages	22. Price*
Unclassified	Unclassified	58	$3.00

*For sale by the National Technical Information Service, Springfield, Virginia 22151

EFFECT OF WING DESIGN ON THE LONGITUDINAL AERODYNAMIC CHARACTERISTICS OF A WING-BODY MODEL AT SUBSONIC SPEEDS

By William P. Henderson and Jarrett K. Huffman
Langley Research Center

SUMMARY

An investigation has been conducted to determine the effects of wing camber and twist on the longitudinal aerodynamic characteristics of a wing-body configuration. Three wings were used, each having the same planform (aspect ratio of 2.5 and leading-edge sweep angle of 44°) but differing in amounts of camber and twist (wing design lift coefficient $C_{L,d}$). The wing design lift coefficients were 0, 0.35, and 0.70. The investigation was conducted over a Mach number range from 0.20 to 0.70 at angles of attack up to about 22°. The effect of wing strakes on the aerodynamic characteristics of the cambered wings was also studied. A comparison of the experimentally determined aerodynamic characteristics with theoretical estimates is also included.

The results indicate that increasing wing camber and twist result in a significant increase in maximum lift coefficient, a nose-down pitching-moment-coefficient increment, an increase in drag at low lift coefficients, and a reduction in drag at the higher lift coefficients. Variations in Mach number and Reynolds number did not significantly alter the aerodynamic characteristics of the uncambered wing ($C_{L,d} = 0$). As the design lift coefficient was increased, however, Mach number and Reynolds number effects became considerably more pronounced. Adding the wing strake to the uncambered wing results in a slight reduction in stability level, a large increase in lift, and a decrease in drag at the higher lift coefficients. As the camber and twist (wing design lift coefficient) are increased, the lift associated with adding the wing strake is reduced. The estimated analytical aerodynamic characteristics for the uncambered wing with the strake agree reasonably well with the experimental data when the vortex lift is considered in the calculations.

INTRODUCTION

The National Aeronautics and Space Administration is currently conducting wind-tunnel investigations to provide information for use in developing fighter airplanes

possessing desirable stability, control, and performance characteristics at the higher maneuvering lift coefficients.

The present paper discusses a study of two concepts for achieving high lift-drag ratios at maneuvering lift coefficients. The first is to design the wing camber and twist to support a load distribution for which the extent of regions of adverse pressure gradient is minimized; thus, the tendency for flow separation at the design lift coefficients is suppressed. This concept was investigated for a range of design lift coefficients up to 0.7. The use of leading- and trailing-edge flaps to approximate this concept was investigated in reference 1.

The second concept makes use of the vortex lift produced by leading-edge separation from sharp highly swept wing strakes. The success of this concept depends on the mutual interaction of the strake vortex and the main wing which is difficult to predict analytically. These two concepts were investigated individually and in combination in subsonic wind-tunnel tests using a wing-body model. Experimental lift and drag coefficient characteristics obtained with the wing strake and an uncambered wing are compared with analytical predictions based on the leading-edge-suction analogy of vortex lift.

This study was conducted in the Langley high-speed 7- by 10-foot tunnel at Mach numbers from 0.20 to 0.70 and at angles of attack up to 22°.

SYMBOLS

The results as presented are referred to the body axis system with the exception of the lift and drag coefficients, which are referred to the wind axis system. The moment reference center was located at a point 65.91 centimeters rearward of the nose (long fuselage) along the model reference lines. (See fig. 1.)

A	aspect ratio
b	wing span, centimeters
C_D	drag coefficient, $\frac{\text{Drag}}{qS}$
ΔC_D	increment in drag associated with addition of wing strake
$C_{D,o}$	drag coefficient at zero lift

C_L lift coefficient, $\frac{\text{Lift}}{qS}$

ΔC_L increment in lift associated with addition of wing strake

$C_{L,d}$ wing design lift coefficient

C_m pitching-moment coefficient, $\frac{\text{Pitching moment}}{qS\bar{c}}$

c local wing chord, centimeters

$\bar{c}$ wing mean geometric chord, 23.30 centimeters

M Mach number

n nth loading function

q free-stream dynamic pressure, newtons per meter^2

R Reynolds number (based on $\bar{c}$)

S wing reference area, 1.0322 meters^2

s leading-edge-suction parameter, $\frac{C_L \tan \alpha - (C_D - C_{D,o})}{C_L \tan \alpha - A \int_{-1}^{1} \Gamma \alpha_i \, d \frac{y}{b/2}}$

x distance behind leading edge of wing, centimeters

y distance from fuselage reference line (measured spanwise), centimeters

z wing airfoil ordinate, centimeters

α angle of attack, degrees

α_i induced angle of attack

Γ circulation strength

θ angle used to locate pressure doublets chordwise, 0 at leading edge and π at trailing edge

Subscripts:

l lower surface

u upper surface

MODEL DESCRIPTION

A three-view drawing of the basic model is presented in figure 1(a) and a drawing showing the model with the wing strake is presented in figure 1(b). A photograph of the model sting mounted in the Langley high-speed 7- by 10-foot tunnel is presented in figure 2. The model as illustrated in figure 1(a) consists of a simple wing-fuselage configuration, with the wing having an aspect ratio of 2.5, a taper ratio of 0.20, a wing leading-edge sweep angle of 44°, and NACA 64A series airfoil sections (measured streamwise) with a thickness ratio of 6 percent at the fuselage juncture and 4 percent at the wing tip. Three variations in wing camber and twist, corresponding to design lift coefficients of 0, 0.35, and 0.70 were studied. Ordinates for the cambered airfoils are presented in table I. Two fuselage lengths were studied; the long fuselage was 11.94 cm longer than the short fuselage. The wing strake (fig. 1(b)) was constructed of a 0.159-cm-thick flat plate with sharp leading edges. The sharp leading edge had a total bevel angle of 3.2°.

WING DESIGN PROCEDURE

The mean camber surfaces of the two cambered and twisted wings were designed by using the procedure of reference 2 for design points corresponding to C_L of 0.35 or 0.70 at a Mach number of 0.40. At the design points, an elliptical span-load distribution was specified and the chordwise load distribution was specified as the superposition of four $\sin n\theta$ pressure modes with $n = 1, 3, 5$, and 7, where

$$\cos \theta = 1 - \frac{2x}{c}$$

The magnitude of the modes at each spanwise station was selected to approximate a rectangular chordwise load distribution. The resulting distribution is characterized by zero load at the leading edge and a very small region of strong adverse pressure gradient in the vicinity of the trailing edge. No camber was incorporated in the fuselage.

TEST AND CORRECTIONS

The investigation was conducted in the Langley high-speed 7- by 10-foot tunnel at Mach numbers from 0.20 to 0.70 and at angles of attack up to 22°. The variation of the test Reynolds number, based on the wing mean geometric chord, with Mach number is presented in figure 3. Transition strips 0.32 cm wide of No. 100 carborundum grains (based on analysis of ref. 3) were placed 1.14 cm streamwise from the leading edge of the wings and 2.54 cm behind the nose of the fuselage.

Corrections to the model angle of attack have been made for deflections of the balance and sting support system due to aerodynamic load. Pressure measurements obtained from orifices located within the fuselage base cavity were used to adjust the drag coefficient to a condition of free-stream static pressure at the model base.

Jet-boundary and blockage corrections estimated by the procedures of references 4 and 5, respectively, were applied to the data.

PRESENTATION OF RESULTS

The basic longitudinal aerodynamic characteristics are presented in figures 4 to 10 and pertinent results are summarized in figures 11 and 12. As an aid in locating a particular part of the data, the following list of figures is presented:

RESULTS AND DISCUSSION

The effect of wing camber and twist on the longitudinal aerodynamic characteristics of the wing-body configuration at Mach numbers from 0.20 to 0.70 is presented in figure 4. An analysis of the effect of camber on the drag due to lift is presented in figure 5 and the combined effects of Mach number and Reynolds number on the aerodynamic characteristics of the model are presented in figure 6. Increasing the wing camber and twist ($C_{L,d}$) results in a significant increase in the maximum lift coefficient obtained, with essentially no change in lift-curve slope between the uncambered and moderately cambered wing ($C_{L,d} = 0.35$). The highly cambered wing ($C_{L,d} = 0.70$) showed some nonlinearity in lift-curve slope over most of the angle-of-attack range; thus, the presence of flow separation on the wing was indicated.

Increasing the wing camber and twist ($C_{L,d}$) is shown in figure 4 to result in relatively large values of nose-down pitching moment with some slight change in the pitching-moment-coefficient curve slope in the low lift coefficient range. The nose-down pitch could result in trim drag problems for an airplane configuration, unless careful attention is given to the location of the center of gravity of the airplane and to the size of the longitudinal control surface.

At the higher lift coefficients the uncambered wing ($C_{L,d} = 0$) shows a severe increase in stability (pitch down) which is eliminated as the wing design lift coefficient is increased.

The drag characteristics illustrated in figure 4 show that cambering the wing, as would be expected, results in a significant increase in the drag at zero lift coefficient and a considerable reduction in drag at the higher lift coefficients. Figure 5 presents an analysis of the effects of camber on the drag characteristics, in that the drag of each wing is compared with the zero and full leading-edge-suction boundaries (lower part of fig. 5). The percent leading-edge suction developed by each wing is also presented for comparison purposes in this figure. The two theoretical boundaries and the equation for computing leading-edge suction are discussed in reference 6. The leading-edge-suction parameter s as presented here simply represents the location of the experimental drag data relative to the two theoretical boundaries. For simplicity, only the zero leading-edge-suction boundary for the uncambered wing is presented in figure 5. The zero leading-edge-suction boundaries for the cambered wings would be essentially the same in the low lift range as that presented in figure 5. At the higher lift coefficients, the zero leading-edge-suction boundaries for the cambered wings would be slightly lower because of the improved lift-curve slope exhibited by the cambered wings. The data obtained on the uncambered wing model, because of extensive leading-edge separation, depart from the full suction boundary at a relatively low lift coefficient. The

cambered wings, however, maintain nearly full leading-edge suction over a fairly wide lift coefficient range. For example, the wing with a design lift coefficient of 0.35 exhibits higher than 90 percent suction over a range of lift coefficients from about 0.25 to 0.60 (fig. 5(b)), whereas the wing with a design lift coefficient of 0.70 maintains over 90 percent suction up to a lift coefficient of nearly 0.90.

The combined effects of Mach number and Reynolds number on the aerodynamic characteristics for the cambered wings of this study are presented in figure 6. Figure 3 presents the variation of Reynolds number with Mach number. The effects of Mach number and Reynolds number cannot be determined independently during these tests since the Langley 7- by 10-foot high-speed tunnel is an atmospheric tunnel and variations in Mach number are accompanied by changes in Reynolds number. The uncambered wing (fig. 6) shows a slight change in the longitudinal aerodynamic characteristics with increasing Mach number and Reynolds number. The most significant effect appears to be in the decrease in the maximum lift coefficient (fig. 6(a)) and the high angle-of-attack nose-down pitching-moment characteristics (fig. 6(c)).

As the design lift is increased (increased camber and twist), the effects of Mach number and Reynolds number are considerably more pronounced. For example, increasing the Mach number and Reynolds number on the highly cambered wing ($C_{L,d} = 0.70$) evidently reduces the extensive flow separation on the wing which, as shown in figure 6, results in a large increase in lift, a decrease in drag, and a nose-down pitching-moment increment.

The effect of fuselage forebody length on the aerodynamic characteristics of the model is illustrated by the data presented in figure 7. Lengthening the forebody, which was necessary to accommodate the wing strake (fig. 1(b)), increased the drag slightly (increased wetted area) and reduced the stability level by about 2 percent $\bar{c}$. The increased wetted area accounted for more than half the drag obtained for the longer fuselage forebody. The effect of forebody length is presented only for the highly cambered wing ($C_{L,d} = 0.70$). It is believed, however, that the effect illustrated for the highly cambered wing would be essentially the same for the other wings of this study.

The effect of adding a wing strake in combination with the cambered wings on the aerodynamic characteristics of the model is presented in figures 8 to 10 and summarized in figure 11. Adding the wing strake (fig. 8) has essentially no effect on the lift coefficient in the low angle-of-attack range (up to about 5°). The increase in lift coefficient expected as a result of the added area of the wing strake is probably compensated for by a detrimental interference effect of the flow field generated by the strake on the wing. At the higher angles of attack adding the wing strake results in a large increase in lift coefficient. This increased lift is the result of the vortex lift generated by the wing

strake (for a discussion of vortex lift, see ref. 7), and according to unpublished flow visualization photographs, the stable vortex system enables the wing to maintain attached flow to a higher angle of attack than the wing without the strake.

Adding the wing strake resulted in a small increase in drag at low lift coefficients, about the level expected due to the added wetted area of the strake. At the highest lift coefficients the vortex lift on the strake and the improved flow conditions on the wings combine to result in a significant decrease in drag. The effect of adding the wing strake on the stability characteristics is discussed subsequently.

A summary of the effect of wing strake on the lift and drag characteristics of the cambered wing design is presented in figure 11. As the flow conditions on the wing are improved by increasing the camber and twist, the increment in lift coefficient associated with adding the wing strake is reduced. This reduction is not surprising since, as previously discussed, part of the lift increment obtained on the flat wing was due to the strake improving the flow conditions on the wing. The beneficial effect of adding the wing strake on the drag due to lift is delayed to a higher lift coefficient as the wing camber and twist (design lift coefficient) are increased. It is evident from these data that, at the intermediate lift coefficients, adding the wing strake resulted in a significant increase in drag, more than would be expected from the increased wetted area. In this intermediate lift range the flow induced on the wing by the strake apparently alters the span-load distribution on the basic wing and gives the resulting drag increase. This result should be expected since the camber and twist for the wing were designed for the wing alone and did not include the strake. Consideration of the strake in the basic wing design could possibly eliminate this large drag increase.

As previously discussed, the basic wing ($C_{L,d} = 0$) exhibits linear pitching-moment characteristics (fig. 8) up to the angle of attack for wing stall. Above this angle of attack, the wing shows a large stable break (pitch down) in the pitching-moment characteristics. When the basic wing, with its pitch-down characteristics, is combined with the wing strake which should contribute a pitch-up tendency, the resulting pitching-moment characteristics are reasonably linear throughout the test lift-coefficient range. Adding the wing strake, which adds lifting area ahead of the moment reference center, causes a rather large destabilizing shift in the longitudinal stability level.

A comparison of the estimated and experimentally determined lift and drag characteristics for the uncambered wing ($C_{L,d} = 0$) with the wing strake is presented in figure 12. The estimates were made by using the procedures outlined in reference 8 and included only the vortex lift on the strake. Applying the suction analogy to the entire strake and wing leading edge was found to overpredict the lift characteristics, which should be expected since low-sweep wings generally do not produce much vortex lift. The experimental drag polar appears to show that some leading-edge suction is being developed by

the wing even at the higher lift coefficients. On the whole, the estimated analytical aerodynamic characteristics for the uncambered wing with the strake agree reasonably well with the experimental data when the strake vortex lift is considered in the calculations.

CONCLUSIONS

A wind-tunnel study has been made to determine the effects of wing camber and twist on the longitudinal aerodynamic characteristics of a wing-body configuration. As a result of this program several conclusions can be made:

1. Increasing the wing camber and twist results in a significant increase in the maximum lift coefficient, a nose-down pitching-moment-coefficient increment, an increase in drag at low lift coefficient, and a reduction in the drag at the higher lift coefficients.

2. Variation in Mach number and Reynolds number did not significantly alter the aerodynamic characteristics of the uncambered wing. As the design lift coefficient was increased, however, Mach number and Reynolds number effects became considerably more pronounced.

3. Adding the wing strake to the uncambered wing results in a slight reduction in the stability level and a large increase in the lift and a decrease in drag at the higher lift coefficient. As the camber and twist are increased the lift increase associated with adding the wing strake is reduced.

4. The estimated analytical aerodynamic characteristics for the uncambered wing with the strake agree reasonably well with the experimental data when the strake vortex lift is considered in the calculations.

Langley Research Center,
National Aeronautics and Space Administration,
Hampton, Va., October 31, 1972.

REFERENCES

1. Henderson, William P.; and Graves, Ernald B.: Subsonic and Supersonic Longitudinal Characteristics of a Fighter Model With Wing-Mounted Nacelles and Leading- and Trailing-Edge Flaps. NASA TM X-2105, 1971.

2. Lamar, John E.: A Modified Multhopp Approach for Predicting Lifting Pressures and Camber Shape for Composite Planforms in Subsonic Flow. NASA TN D-4427, 1968.

3. Braslow, Albert L.; Hicks, Raymond M.; and Harris, Roy V., Jr.: Use of Grit-Type Boundary-Layer-Transition Trips on Wind-Tunnel Models. NASA TN D-3579, 1966.

4. Gillis, Clarence L.; Polhamus, Edward C.; and Gray, Joseph L., Jr.: Charts for Determining Jet-Boundary Corrections for Complete Models in 7- by 10-Foot Closed Rectangular Wind Tunnels. NACA WR L-123, 1945. (Formerly NACA ARR L5G31.)

5. Herriot, John G.: Blockage Corrections for Three-Dimensional-Flow Closed-Throat Wind Tunnels, With Consideration of the Effect of Compressibility. NACA Rep. 995, 1950. (Supersedes NACA RM A7B28.)

6. Henderson, William P.: Studies of Various Factors Affecting Drag Due to Lift at Subsonic Speeds. NASA TN D-3584, 1966.

7. Polhamus, Edward C.: A Concept of the Vortex Lift of Sharp-Edge Delta Wings Based on a Leading-Edge-Suction Analogy. NASA TN D-3767, 1966.

8. Polhamus, Edward C.: Application of the Leading-Edge-Suction Analogy of Vortex Lift to the Drag Due to Lift of Sharp-Edge Delta Wings. NASA TN D-4739, 1968.

TABLE I.- ORDINATES OF CAMBERED WING

(a) $C_{L,d} = 0.35$

x/c	$\frac{y}{b/2} = 0.131$ $\frac{c}{\bar{c}} = 1.300$		$\frac{y}{b/2} = 0.259$ $\frac{c}{\bar{c}} = 1.151$		$\frac{y}{b/2} = 0.383$ $\frac{c}{\bar{c}} = 1.009$		$\frac{y}{b/2} = 0.500$ $\frac{c}{\bar{c}} = 0.872$		$\frac{y}{b/2} = 0.609$ $\frac{c}{\bar{c}} = 0.745$		$\frac{y}{b/2} = 0.707$ $\frac{c}{\bar{c}} = 0.630$	
	z_u/c	z_l/c	z_u/c	z_l/c	z_u/c	z_l/c	z_u/c	z_l/c	z_u/c	z_l/c	z_l/c	z_l/c
0.00	0.0599	0.0599	0.0518	0.0518	0.0459	0.0459	0.0417	0.0417	0.0370	0.0370	0.0320	0.0320
.03	.0722	.0515	.0640	.0445	.0581	.0396	.0538	.0363	.0490	.0324	.0440	.0280
.05	.0771	.0487	.0692	.0423	.0634	.0380	.0593	.0351	.0546	.0317	.0497	.0278
.08	.0803	.0461	.0727	.0404	.0671	.0365	.0631	.0340	.0586	.0310	.0539	.0275
.10	.0827	.0437	.0753	.0385	.0700	.0351	.0661	.0330	.0618	.0304	.0573	.0272
.15	.0860	.0397	.0793	.0355	.0744	.0329	.0709	.0315	.0670	.0296	.0629	.0271
.20	.0881	.0363	.0821	.0331	.0778	.0313	.0747	.0306	.0712	.0294	.0676	.0276
.25	.0891	.0332	.0838	.0309	.0800	.0299	.0773	.0298	.0743	.0292	.0711	.0280
.30	.0889	.0302	.0842	.0287	.0809	.0283	.0785	.0286	.0759	.0285	.0732	.0279
.35	.0874	.0271	.0833	.0262	.0804	.0263	.0783	.0270	.0761	.0274	.0737	.0270
.40	.0848	.0240	.0812	.0237	.0787	.0242	.0769	.0252	.0750	.0259	.0729	.0260
.45	.0812	.0214	.0781	.0216	.0759	.0224	.0744	.0236	.0728	.0245	.0710	.0249
.50	.0768	.0194	.0742	.0200	.0724	.0210	.0712	.0225	.0699	.0236	.0685	.0242
.55	.0718	.0179	.0698	.0189	.0684	.0201	.0675	.0217	.0665	.0230	.0655	.0239
.60	.0664	.0168	.0649	.0180	.0639	.0194	.0633	.0211	.0626	.0226	.0619	.0237
.65	.0603	.0157	.0592	.0171	.0586	.0187	.0583	.0204	.0579	.0219	.0575	.0231
.70	.0534	.0145	.0527	.0160	.0524	.0175	.0523	.0193	.0521	.0208	.0519	.0220
.75	.0457	.0130	.0453	.0145	.0452	.0159	.0452	.0175	.0457	.0193	.0452	.0200
.80	.0375	.0112	.0373	.0125	.0373	.0138	.0375	.0152	.0376	.0164	.0376	.0174
.85	.0291	.0094	.0292	.0105	.0293	.0116	.0295	.0128	.0297	.0138	.0299	.0147
.90	.0208	.0075	.0210	.0085	.0213	.0095	.0217	.0105	.0221	.0114	.0224	.0122
.95	.0119	.0052	.0123	.0059	.0127	.0066	.0131	.0074	.0136	.0081	.0139	.0087
1.00	.0001	-.0001	.0001	-.0001	.0001	-.0001	.0001	-.0001	.0001	-.0001	.0001	-.0001

x/c	$\frac{y}{b/2} = 0.793$ $\frac{c}{\bar{c}} = 0.531$		$\frac{y}{b/2} = 0.866$ $\frac{c}{\bar{c}} = 0.445$		$\frac{y}{b/2} = 0.924$ $\frac{c}{\bar{c}} = 0.379$		$\frac{y}{b/2} = 0.966$ $\frac{c}{\bar{c}} = 0.330$		$\frac{y}{b/2} = 0.991$ $\frac{c}{\bar{c}} = 0.300$	
	z_u/c	z_l/c	z_u/c	z_l/c	z_u/c	z_l/c	z_u/c	z_l/c	z_u/c	z_l/c
0.00	0.0258	0.0258	0.0180	0.0182	0.0091	0.0091	0.0010	0.0010	-0.0096	-0.0096
.03	.0377	.0225	.0300	.0154	.0208	.0066	.0104	-.0035	.0015	-.0120
.05	.0437	.0227	.0362	.0159	.0270	.0074	.0167	-.0024	.0079	-.0109
.08	.0480	.0227	.0407	.0164	.0318	.0082	.0217	-.0014	.0131	-.0095
.10	.0516	.0228	.0445	.0168	.0358	.0089	.0260	-.0002	.0178	-.0079
.15	.0577	.0234	.0510	.0181	.0428	.0109	.0337	.0025	.0261	-.0045
.20	.0628	.0245	.0567	.0199	.0490	.0134	.0404	.0056	.0333	-.0008
.25	.0669	.0256	.0612	.0216	.0541	.0157	.0461	.0086	.0395	.0028
.30	.0694	.0261	.0643	.0227	.0579	.0175	.0505	.0111	.0445	.0059
.35	.0704	.0258	.0659	.0231	.0601	.0187	.0536	.0130	.0482	.0085
.40	.0700	.0251	.0660	.0230	.0610	.0192	.0553	.0145	.0506	.0106
.45	.0686	.0244	.0652	.0228	.0608	.0197	.0558	.0157	.0517	.0124
.50	.0665	.0241	.0636	.0228	.0598	.0203	.0554	.0168	.0518	.0140
.55	.0639	.0240	.0614	.0231	.0581	.0210	.0542	.0179	.0509	.0153
.60	.0607	.0240	.0587	.0234	.0558	.0216	.0522	.0188	.0491	.0164
.65	.0566	.0236	.0549	.0232	.0525	.0217	.0492	.0192	.0464	.0170
.70	.0514	.0225	.0500	.0223	.0479	.0211	.0451	.0189	.0427	.0169
.75	.0449	.0206	.0438	.0205	.0422	.0196	.0398	.0178	.0378	.0162
.80	.0375	.0180	.0367	.0180	.0354	.0173	.0336	.0159	.0319	.0146
.85	.0299	.0152	.0293	.0153	.0283	.0146	.0267	.0134	.0253	.0123
.90	.0224	.0126	.0220	.0126	.0210	.0119	.0195	.0106	.0180	.0092
.95	.0141	.0091	.0137	.0090	.0129	.0082	.0144	.0069	.0099	.0055
1.00	.0001	-.0001	.0001	-.0001	.0001	-.0001	.0001	-.0001	.0001	-.0001

TABLE I.- ORDINATES OF CAMBERED WING – Concluded

(b) $C_{L,d} = 0.70$

x/c	$\frac{y}{b/2} = 0.131$ $\frac{c}{\bar{c}} = 1.300$		$\frac{y}{b/2} = 0.259$ $\frac{c}{\bar{c}} = 1.151$		$\frac{y}{b/2} = 0.383$ $\frac{c}{\bar{c}} = 1.009$		$\frac{y}{b/2} = 0.500$ $\frac{c}{\bar{c}} = 0.872$		$\frac{y}{b/2} = 0.609$ $\frac{c}{\bar{c}} = 0.745$		$\frac{y}{b/2} = 0.707$ $\frac{c}{\bar{c}} = 0.630$	
	z_u/c	z_l/c	z_u/c	z_l/c	z_u/c	z_l/c	z_u/c	z_l/c	z_u/c	z_l/c	z_u/c	z_l/c
0.00	0.1198	0.1198	0.1037	0.1037	0.0919	0.0919	0.0835	0.0835	0.0740	0.0740	0.0640	0.0640
.03	.1340	.1134	.1183	.0988	.1069	.0884	.0988	.0813	.0897	.0731	.0799	.0641
.05	.1399	.1116	.1250	.0981	.1141	.0887	.1065	.0823	.0978	.0749	.0885	.0666
.08	.1435	.1093	.1292	.0969	.1189	.0882	.1117	.0826	.1035	.0758	.0946	.0682
.10	.1459	.1069	.1323	.0954	.1225	.0876	.1157	.0826	.1079	.0765	.0995	.0694
.15	.1488	.1025	.1366	.0928	.1280	.0865	.1221	.0827	.1153	.0779	.1079	.0721
.20	.1503	.0985	.1397	.0906	.1323	.0858	.1273	.0832	.1215	.0797	.1151	.0752
.25	.1503	.0944	.1411	.0883	.1349	.0848	.1308	.0833	.1261	.0809	.1207	.0775
.30	.1484	.0897	.1406	.0851	.1354	.0828	.1321	.0822	.1282	.0808	.1237	.0784
.35	.1447	.0843	.1381	.0810	.1337	.0796	.1310	.0797	.1278	.0791	.1241	.0775
.40	.1393	.0785	.1337	.0762	.1301	.0756	.1280	.0763	.1254	.0763	.1223	.0754
.45	.1325	.0728	.1280	.0715	.1251	.0715	.1235	.0727	.1214	.0732	.1190	.0729
.50	.1249	.0675	.1214	.0671	.1192	.0678	.1181	.0693	.1166	.0703	.1149	.0706
.55	.1167	.0628	.1142	.0632	.1127	.0644	.1122	.0663	.1113	.0678	.1102	.0686
.60	.1079	.0584	.1063	.0594	.1055	.0611	.1055	.0634	.1052	.0652	.1047	.0665
.65	.0982	.0537	.0974	.0553	.0972	.0573	.0976	.0598	.0979	.0619	.0978	.0635
.70	.0873	.0484	.0871	.0503	.0873	.0525	.0880	.0550	.0886	.0572	.0889	.0589
.75	.0750	.0424	.0752	.0443	.0757	.0464	.0766	.0488	.0773	.0509	.0778	.0526
.80	.0618	.0356	.0622	.0375	.0629	.0394	.0638	.0415	.0646	.0434	.0651	.0449
.85	.0483	.0286	.0490	.0303	.0497	.0320	.0507	.0339	.0515	.0356	.0522	.0370
.90	.0349	.0217	.0358	.0233	.0367	.0248	.0378	.0265	.0388	.0281	.0396	.0294
.95	.0205	.0138	.0214	.0150	.0223	.0163	.0234	.0177	.0244	.0190	.0253	.0200
1.00	.0001	-.0001	.0001	-.0001	.0001	-.0001	.0001	-.0001	.0001	-.0001	.0001	-.0001

x/c	$\frac{y}{b/2} = 0.793$ $\frac{c}{\bar{c}} = 0.531$		$\frac{y}{b/2} = 0.866$ $\frac{c}{\bar{c}} = 0.445$		$\frac{y}{b/2} = 0.924$ $\frac{c}{\bar{c}} = 0.379$		$\frac{y}{b/2} = 0.966$ $\frac{c}{\bar{c}} = 0.330$		$\frac{y}{b/2} = 0.991$ $\frac{c}{\bar{c}} = 0.300$	
	z_u/c	z_l/c	z_u/c	z_l/c	z_u/c	z_l/c	z_u/c	z_l/c	z_u/c	z_l/c
0.00	0.0515	0.0515	0.0364	0.0364	0.0181	0.0181	-0.0021	-0.0021	-0.0194	-0.0194
.03	.0678	.0525	.0528	.0382	.0344	.0202	.0139	.0000	-.0039	-.0175
.05	.0768	.0558	.0623	.0421	.0441	.0246	.0238	.0047	.0062	-.0125
.08	.0834	.0580	.0693	.0450	.0517	.0281	.0318	.0088	.0148	-.0077
.10	.0888	.0599	.0752	.0474	.0581	.0313	.0389	.0127	.0227	-.0031
.15	.0981	.0639	.0856	.0527	.0697	.0378	.0518	.0206	.0368	.0062
.20	.1064	.0682	.0950	.0582	.0802	.0445	.0634	.0286	.0495	.0153
.25	.1131	.0718	.1027	.0631	.0890	.0506	.0734	.0359	.0606	.0238
.30	.1171	.0738	.1079	.0663	.0955	.0552	.0813	.0419	.0696	.0310
.35	.1184	.0739	.1104	.0676	.0995	.0580	.0868	.0463	.0765	.0367
.40	.1175	.0726	.1106	.0675	.1011	.0593	.0901	.0493	.0811	.0411
.45	.1151	.0709	.1092	.0668	.1011	.0599	.0916	.0514	.0837	.0443
.50	.1117	.0693	.1068	.0661	.0998	.0603	.0915	.0529	.0846	.0468
.55	.1078	.0679	.1038	.0654	.0977	.0605	.0903	.0540	.0839	.0484
.60	.1031	.0663	.0997	.0645	.0944	.0602	.0877	.0543	.0818	.0491
.65	.0968	.0637	.0941	.0624	.0895	.0587	.0834	.0533	.0781	.0486
.70	.0883	.0594	.0863	.0585	.0824	.0555	.0771	.0509	.0724	.0467
.75	.0776	.0533	.0760	.0527	.0730	.0504	.0687	.0466	.0647	.0431
.80	.0652	.0457	.0641	.0454	.0617	.0436	.0583	.0406	.0552	.0379
.85	.0524	.0378	.0516	.0376	.0497	.0361	.0468	.0335	.0441	.0310
.90	.0400	.0301	.0393	.0299	.0375	.0284	.0345	.0256	.0317	.0229
.95	.0256	.0206	.0251	.0203	.0234	.0188	.0206	.0160	.0177	.0132
1.00	.0001	-.0001	.0001	-.0001	.0001	-.0001	.0001	-.0001	.0001	-.0001

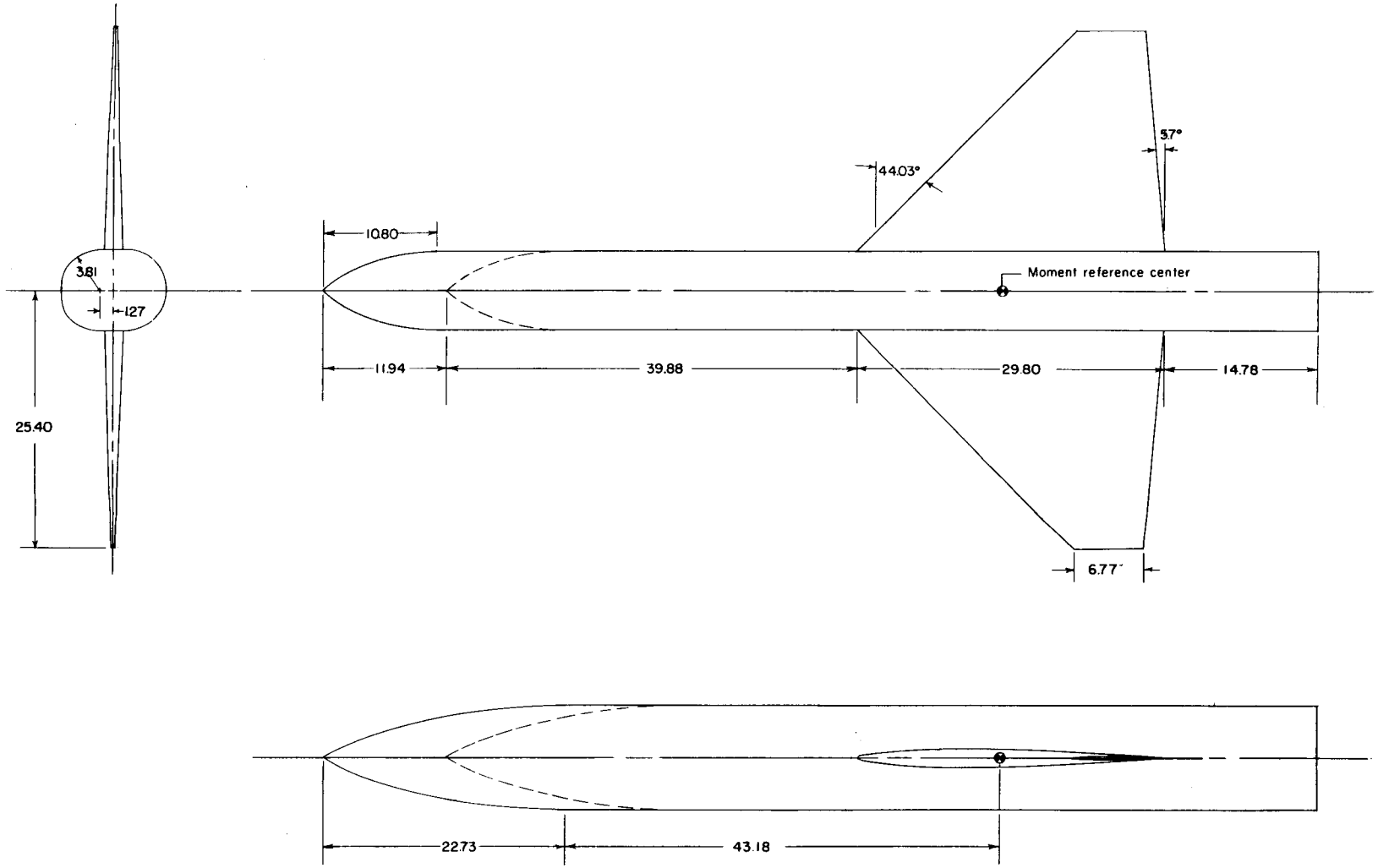

(a) Basic configuration.

Figure 1.- Drawing of the model. Linear dimensions are in centimeters.

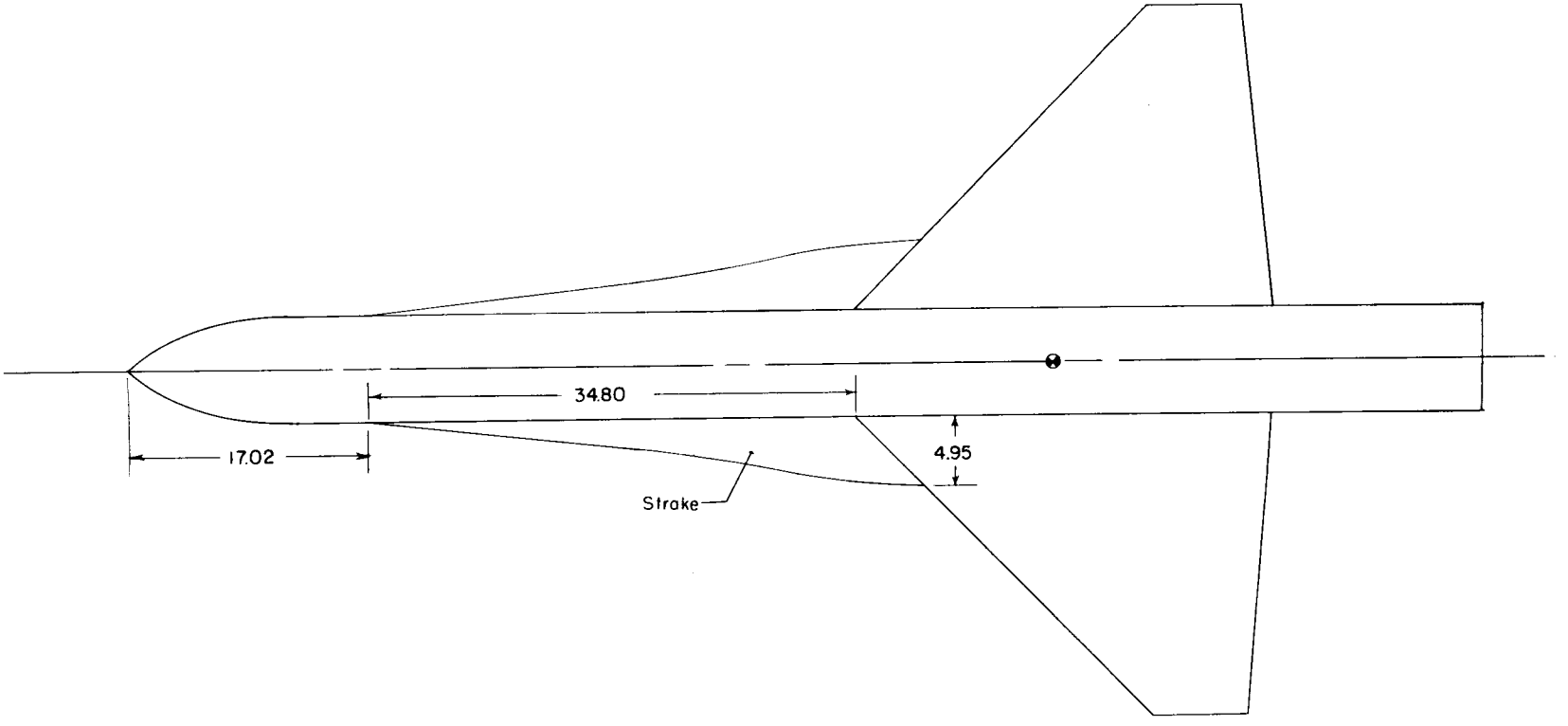

(b) Details of wing strake.

Figure 1.- Concluded.

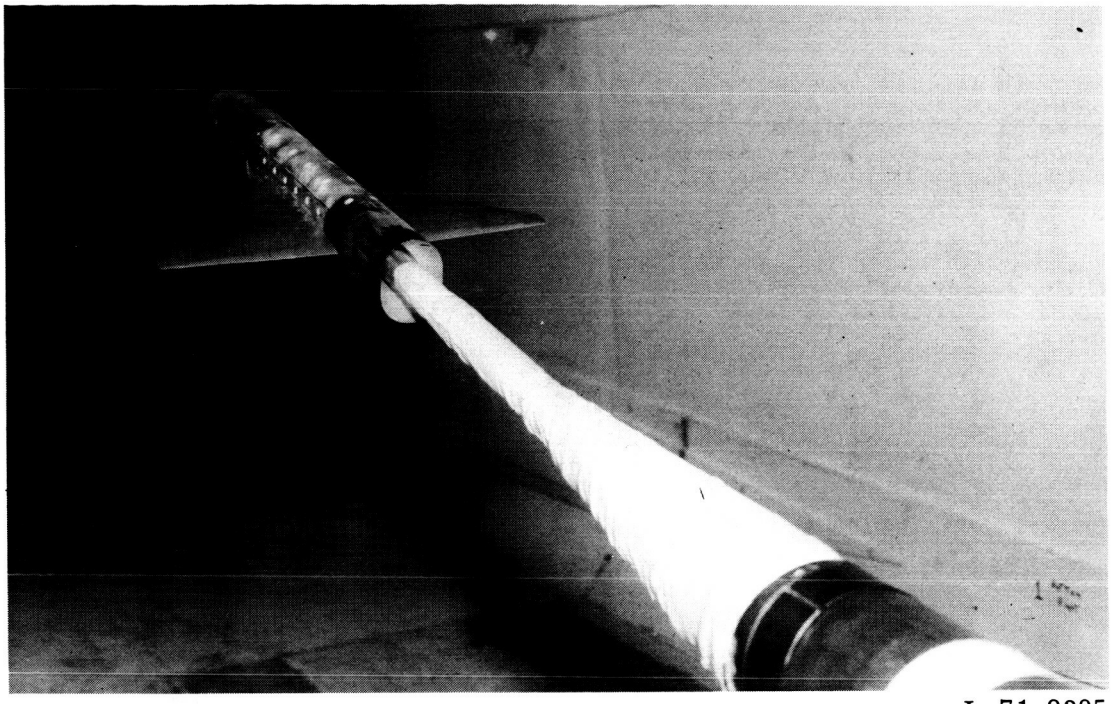

L-71-8385

Figure 2.- Model in Langley high-speed 7- by 10-foot tunnel.

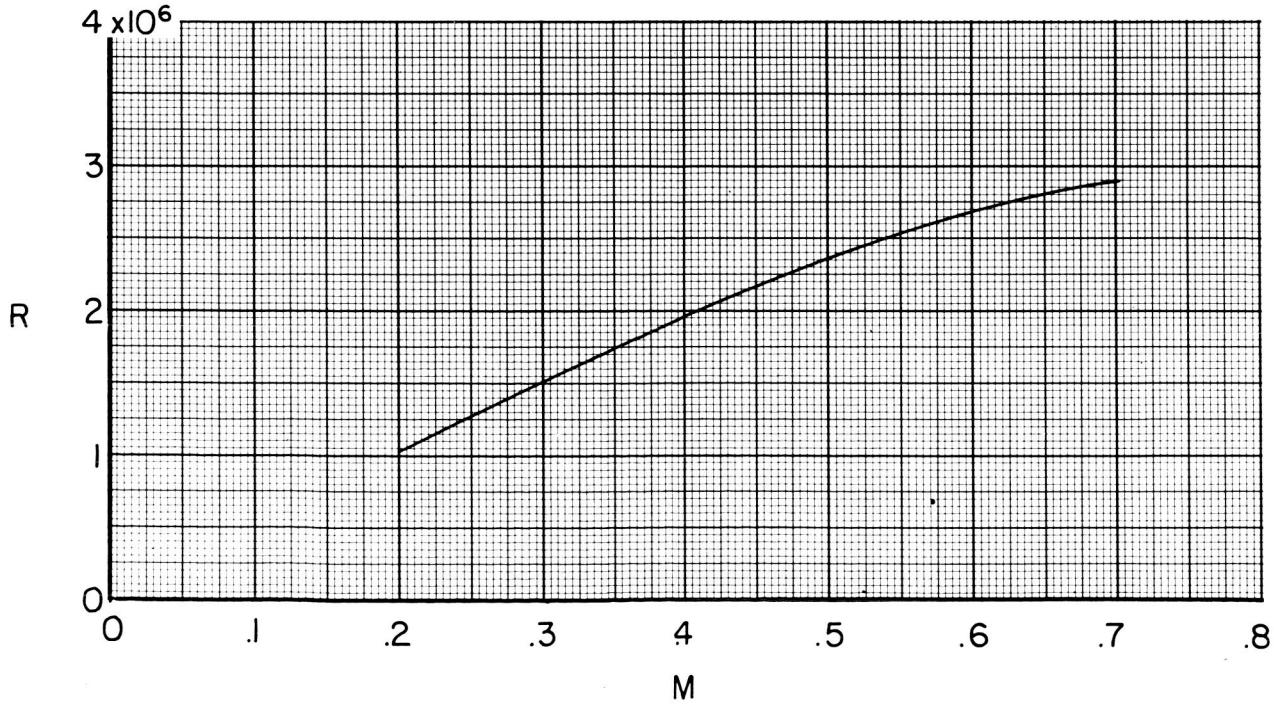

Figure 3.- Variation of test Reynolds number (based on $\bar{c}$) with Mach number.

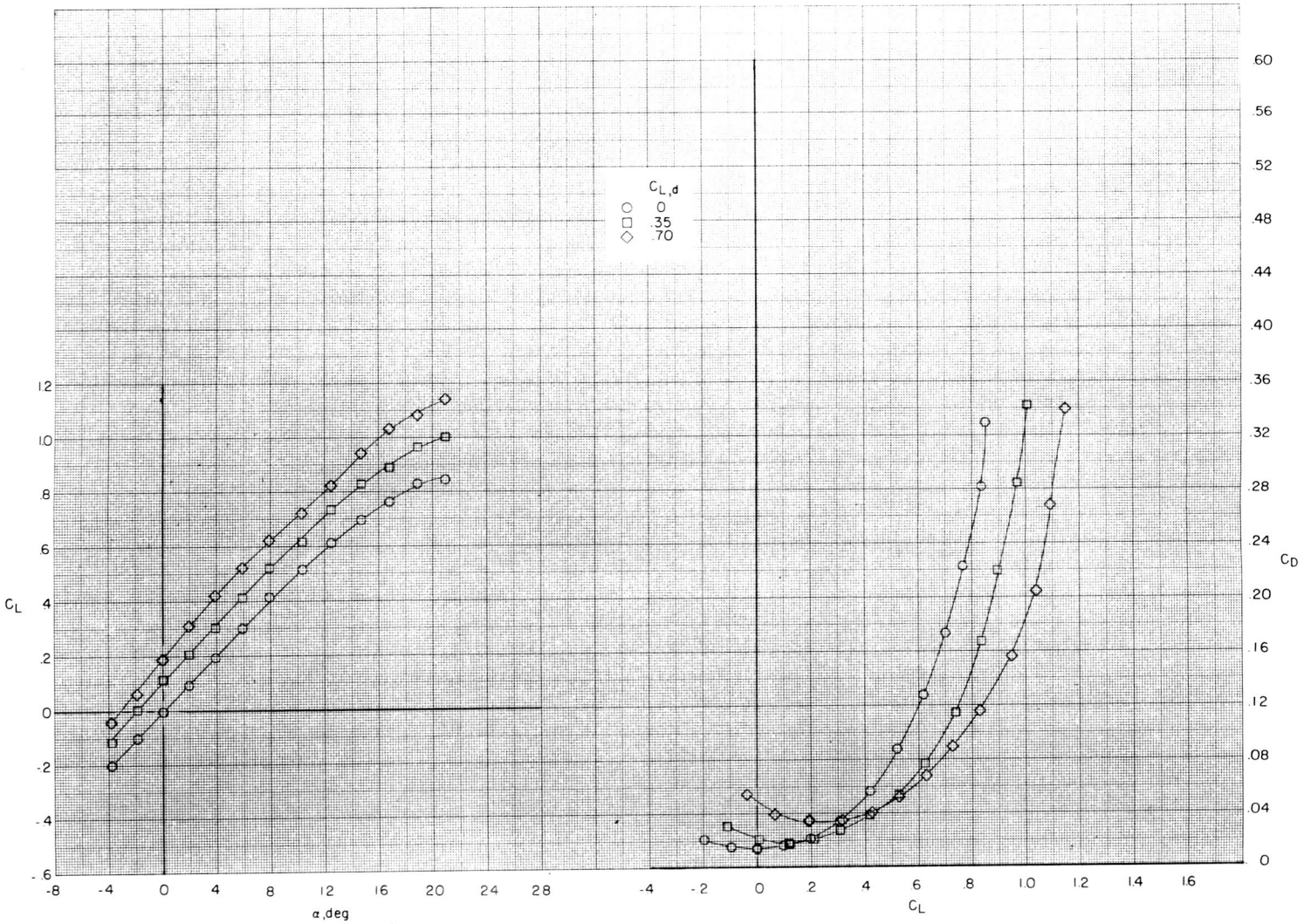

(a) M = 0.20.

Figure 4.- Effect of wing design lift coefficient on aerodynamic characteristics of model with short fuselage forebody and wing strake off.

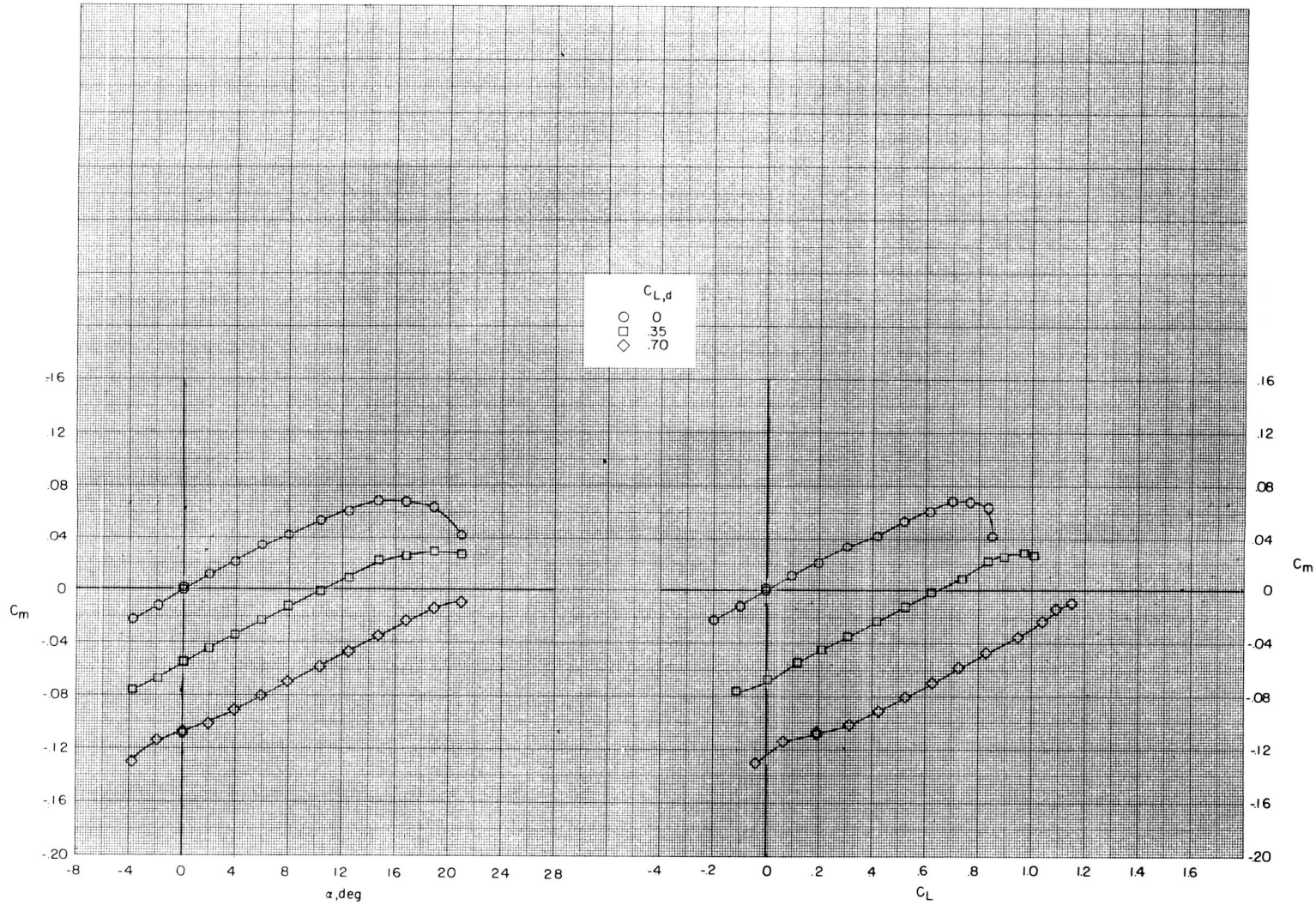

(a) Concluded.

Figure 4.- Continued.

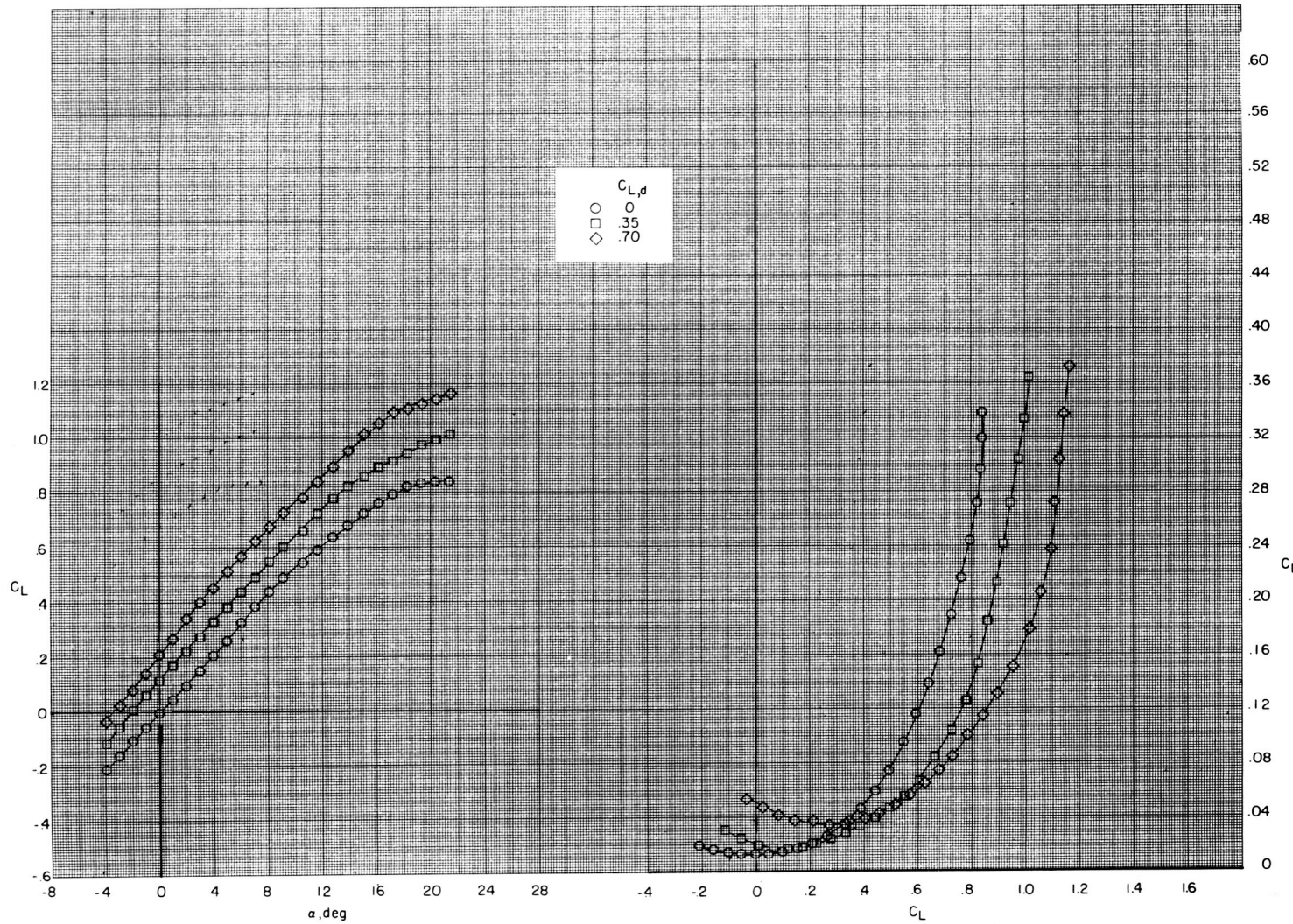

(b) M = 0.40.

Figure 4.- Continued.

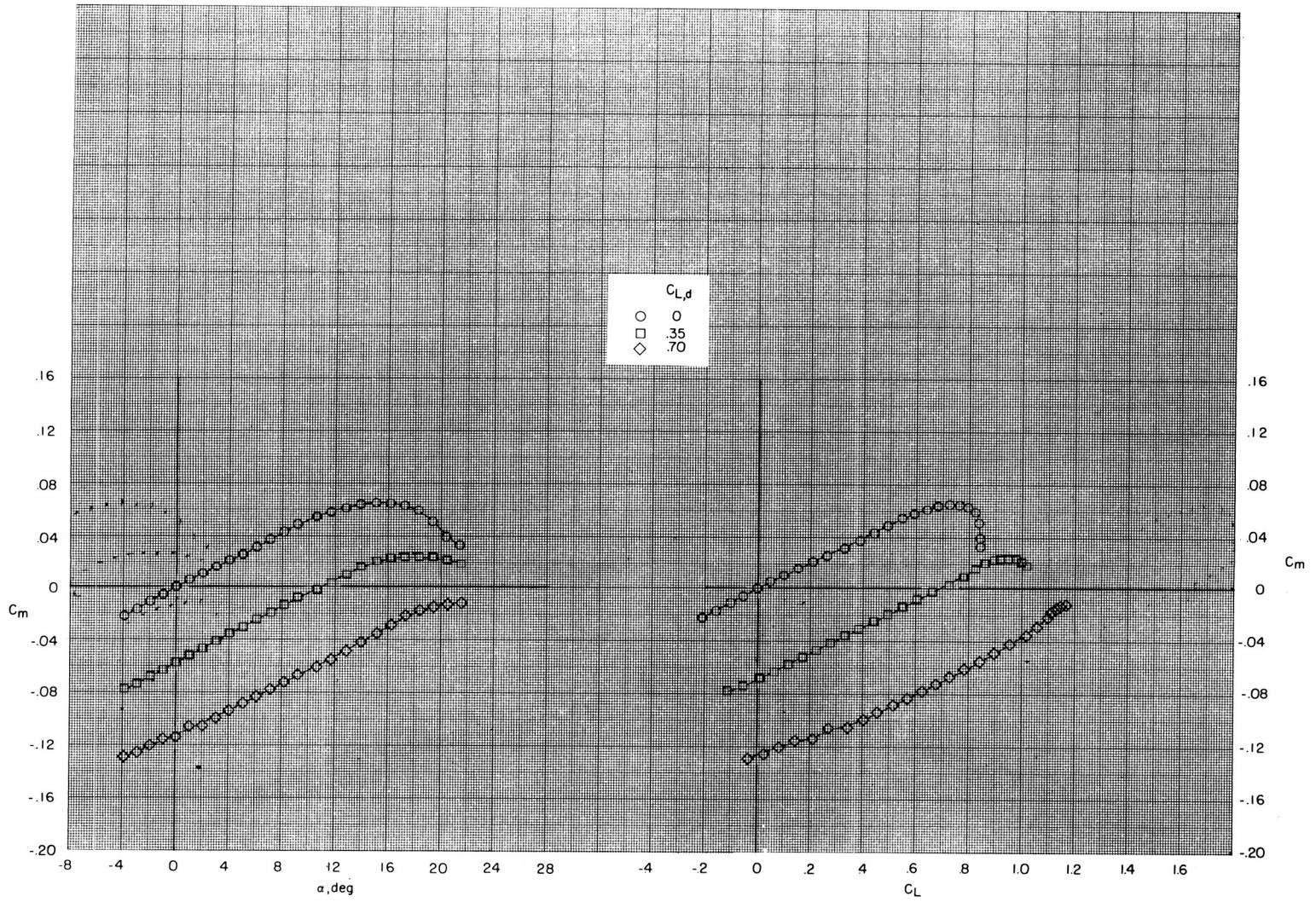

(b) Concluded.

Figure 4.- Continued.

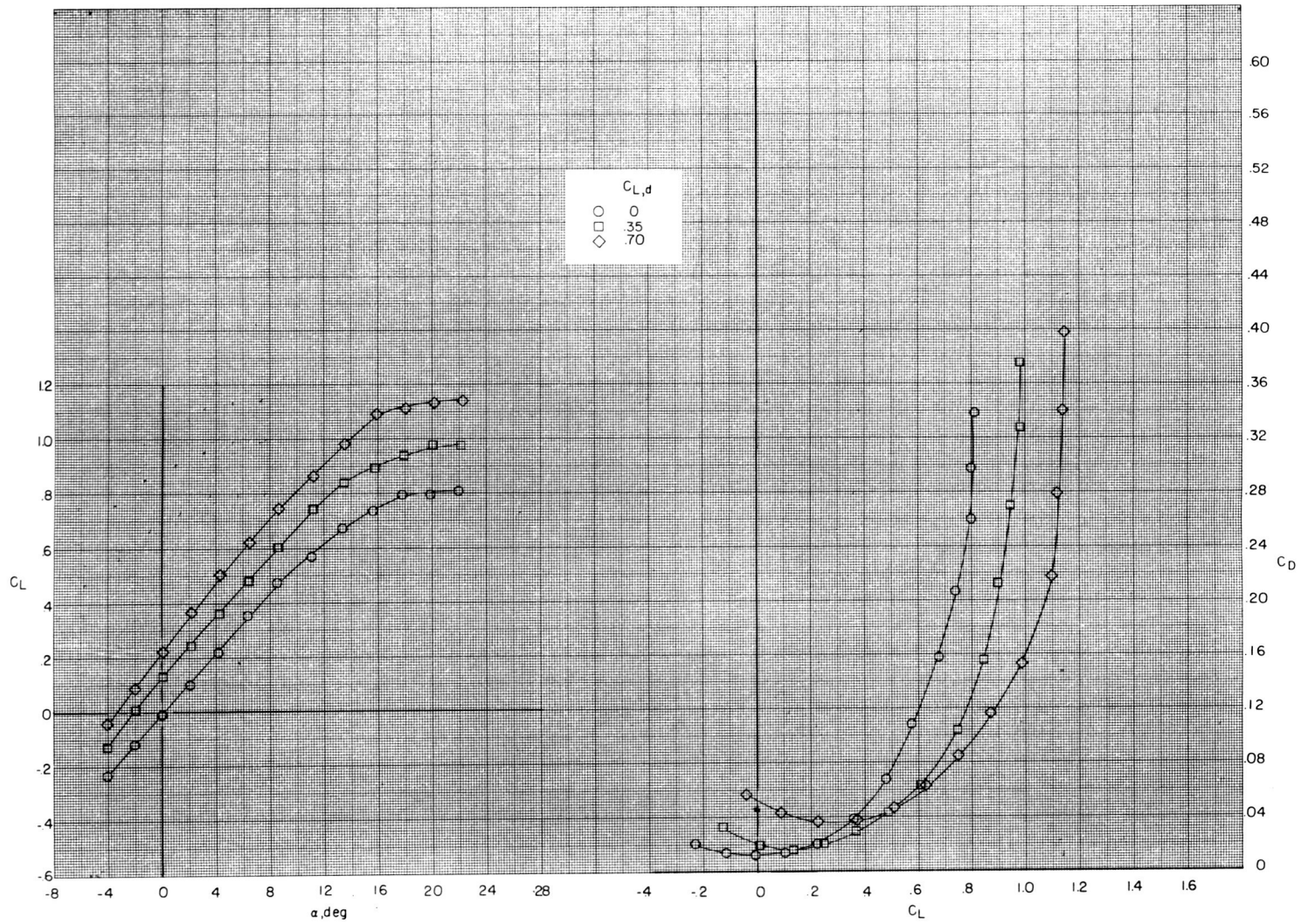

(c) M = 0.60.

Figure 4.- Continued.

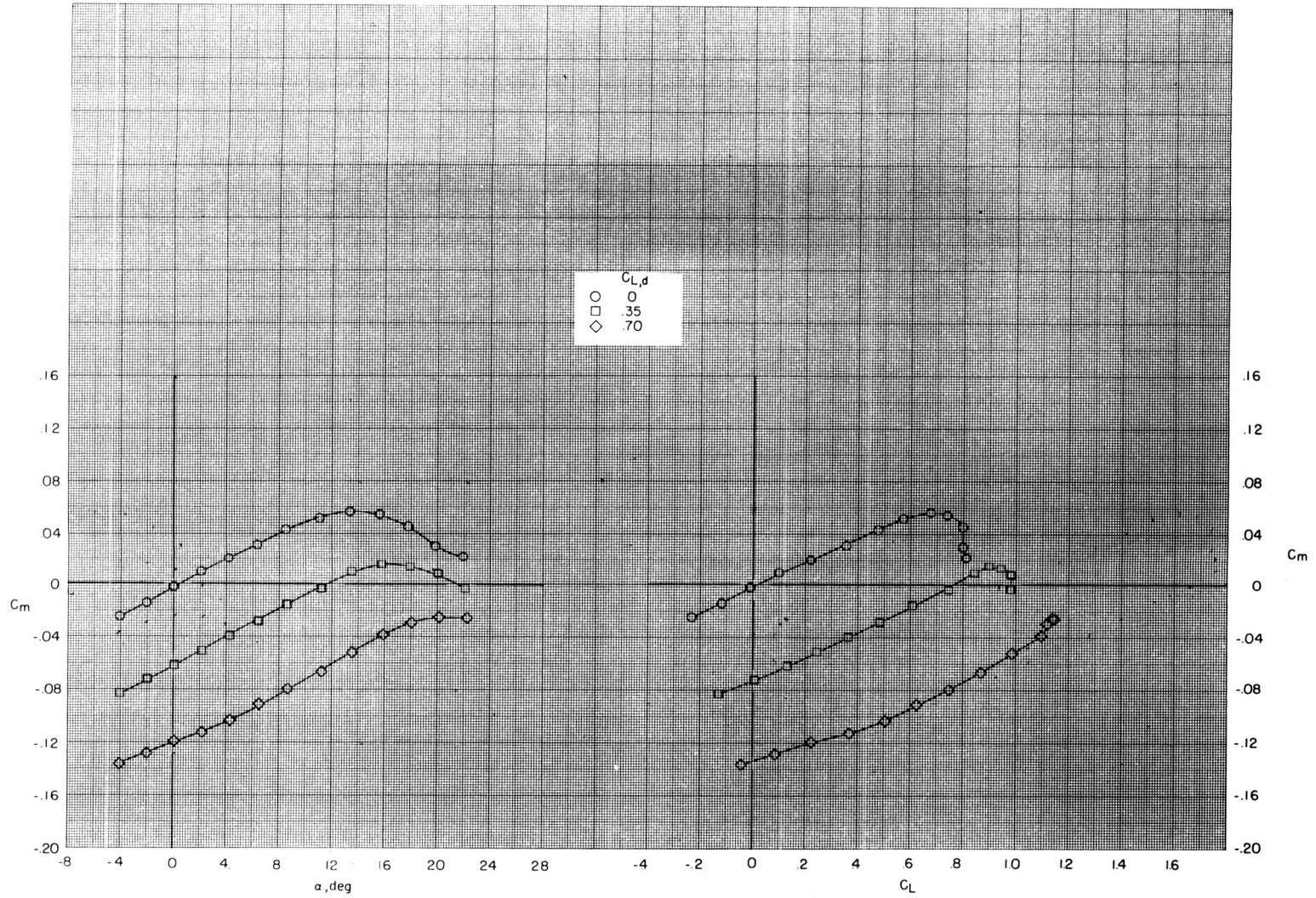

(c) Concluded.

Figure 4.- Continued.

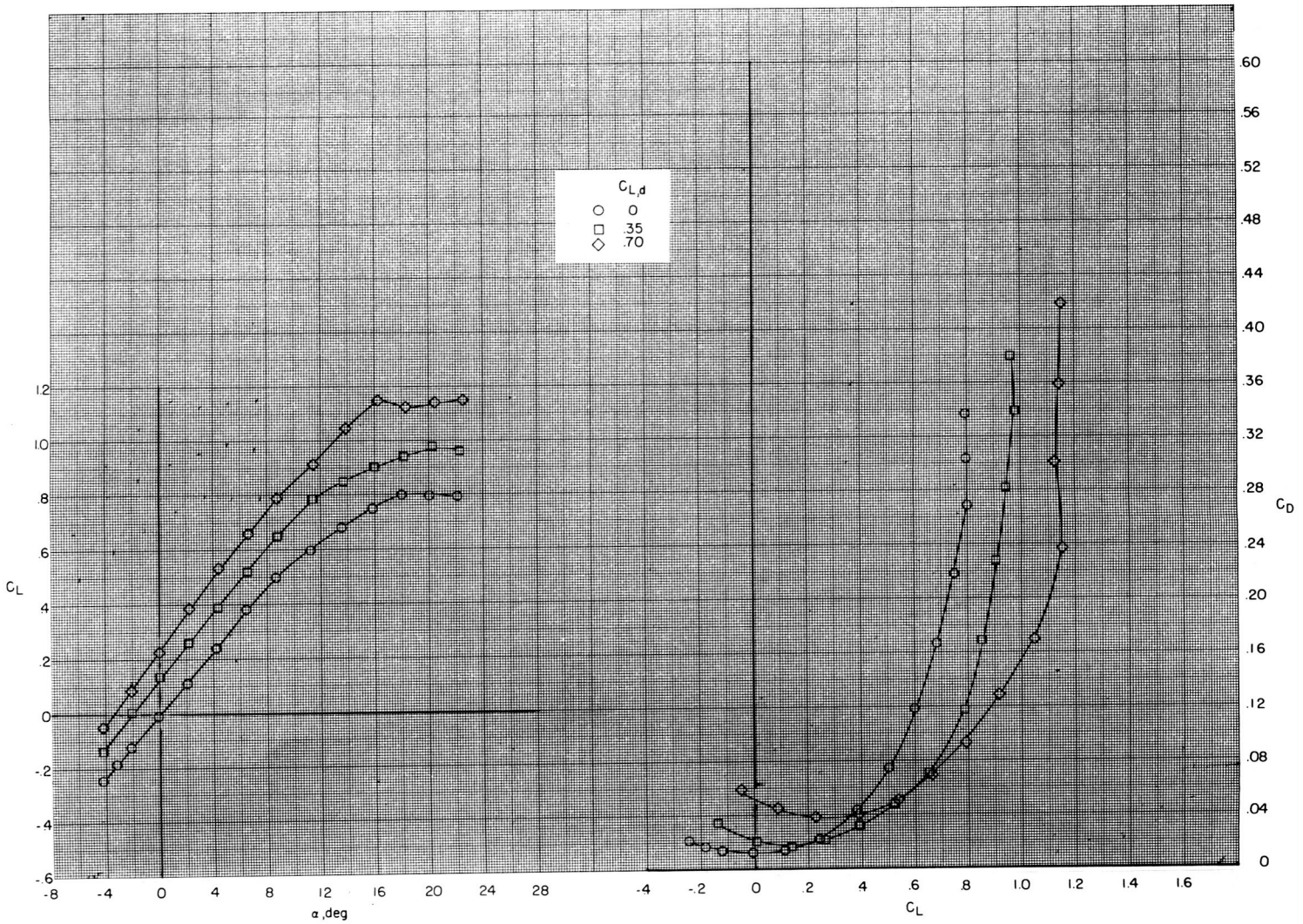

(d) M = 0.70.

Figure 4.- Continued.

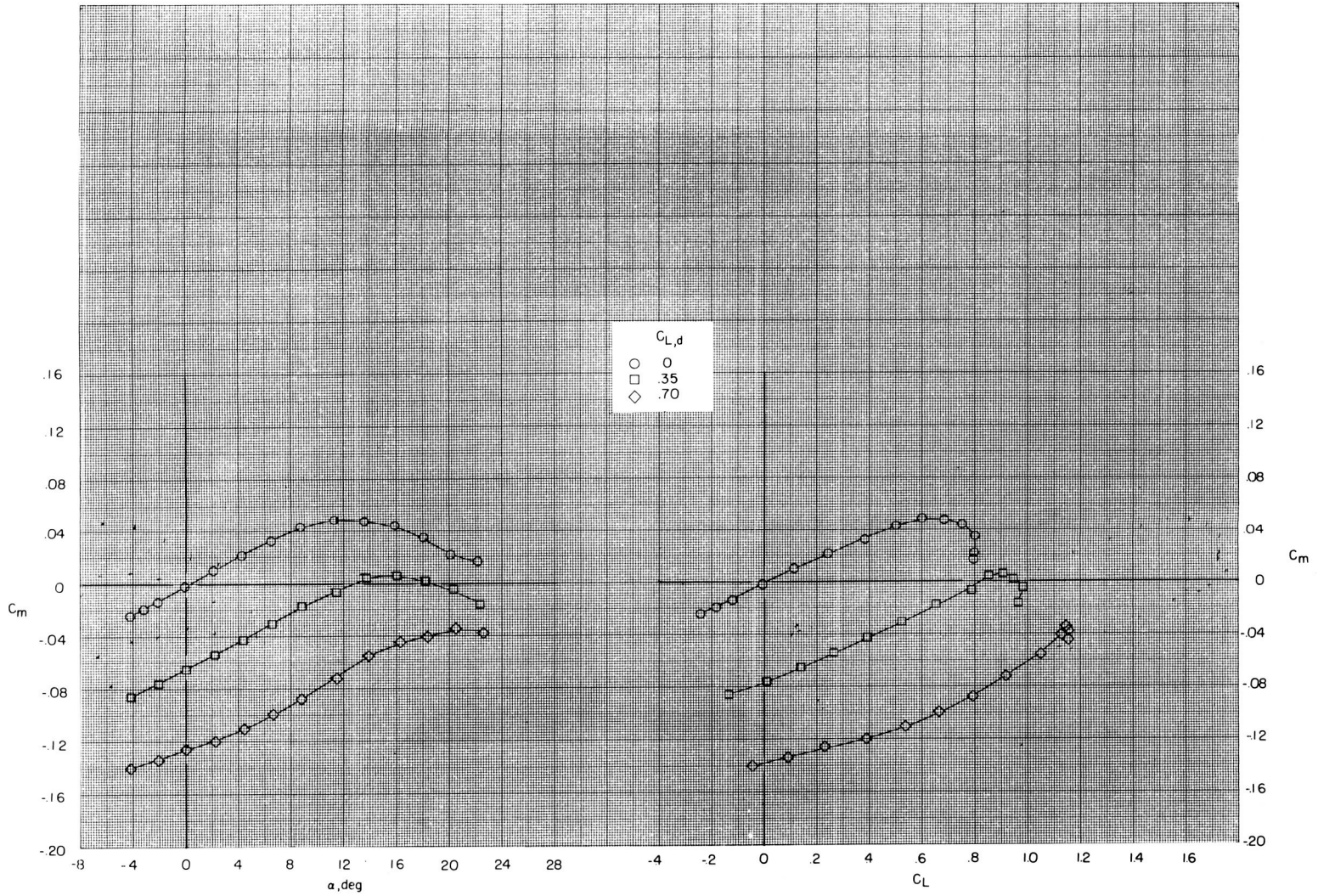

(d) Concluded.

Figure 4.- Concluded.

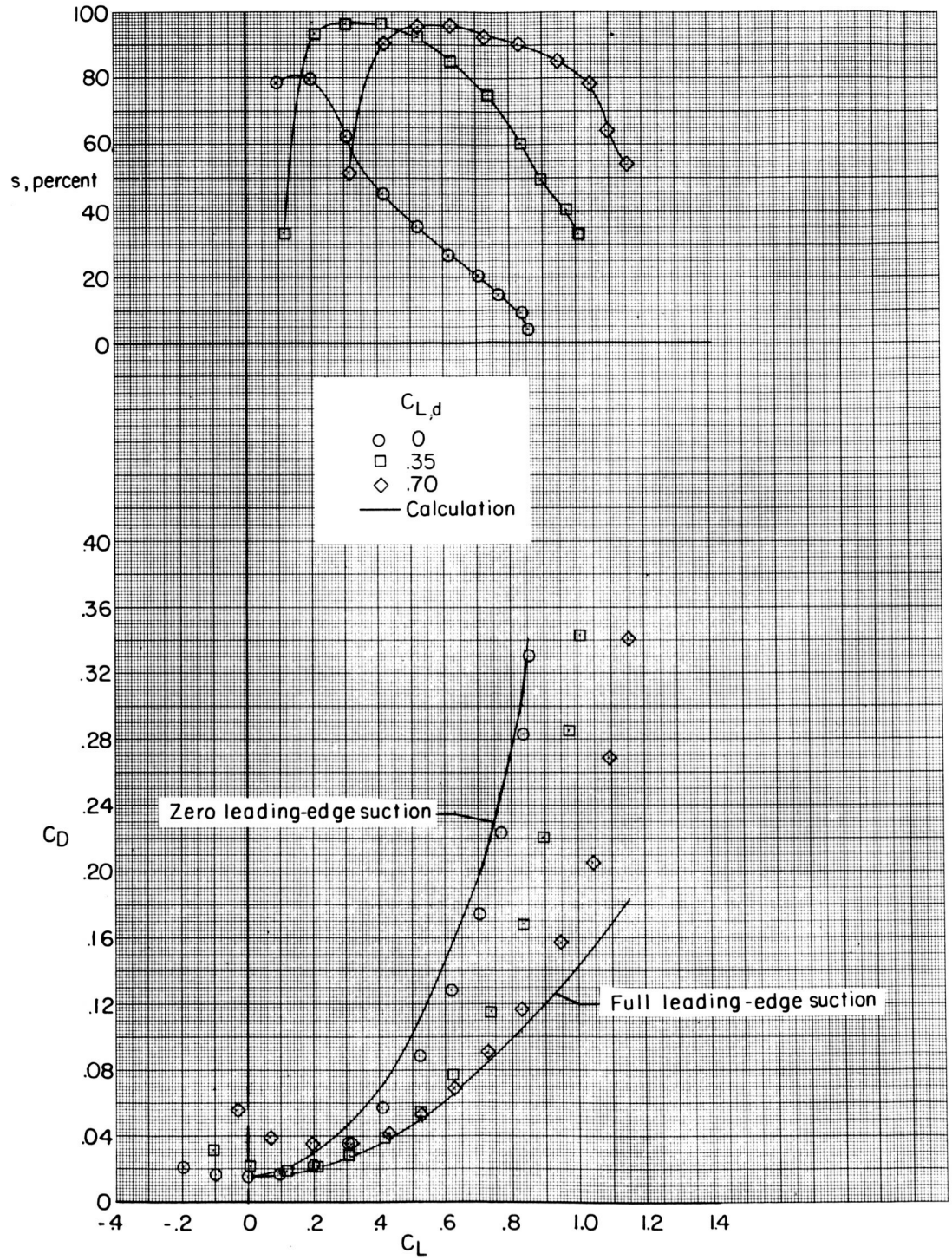

(a) M = 0.20.

Figure 5.- Effect of wing design lift coefficient on drag due to lift characteristics of model with short fuselage forebody and wing strake off.

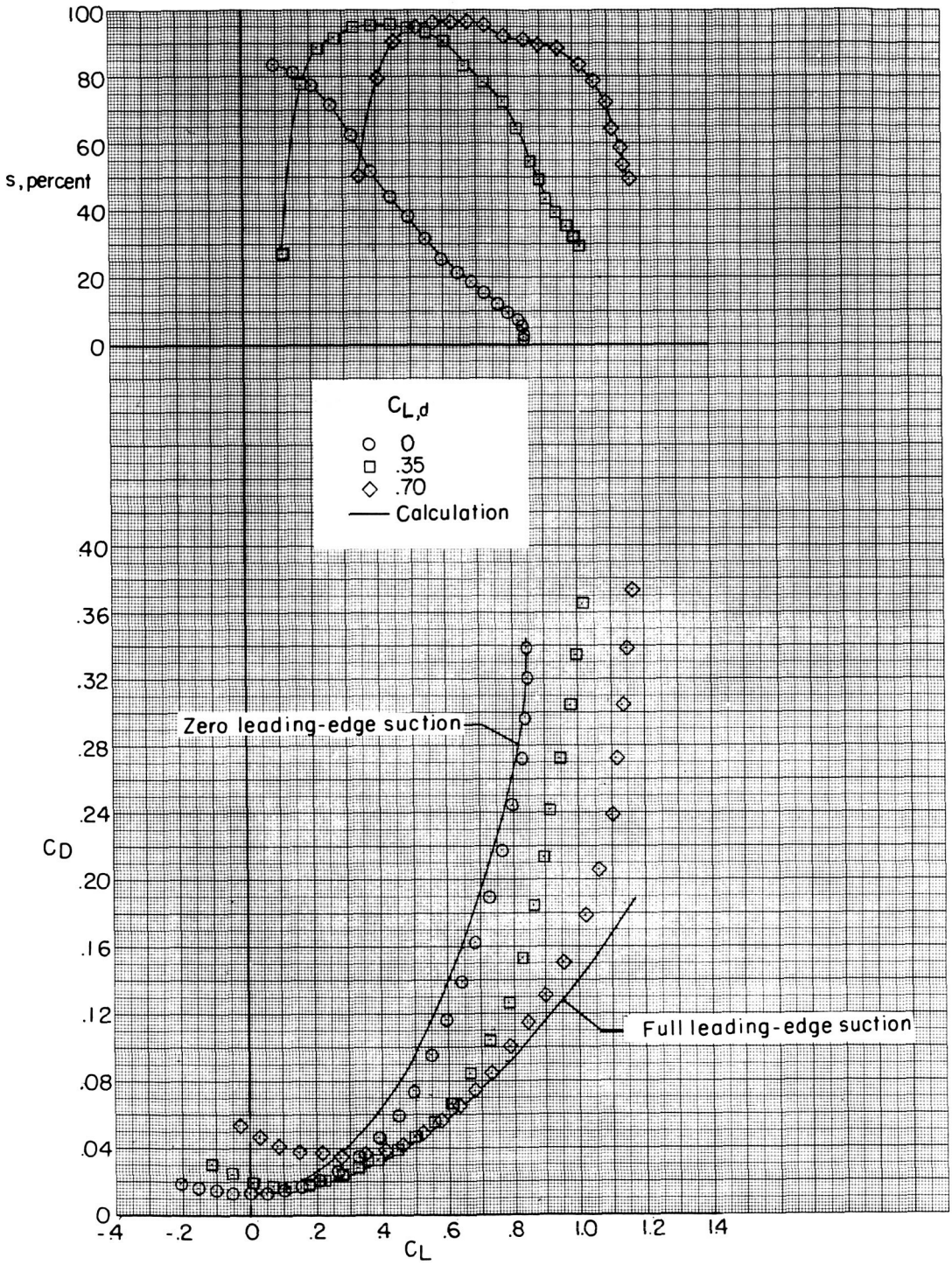

(b) M = 0.40.

Figure 5.- Continued.

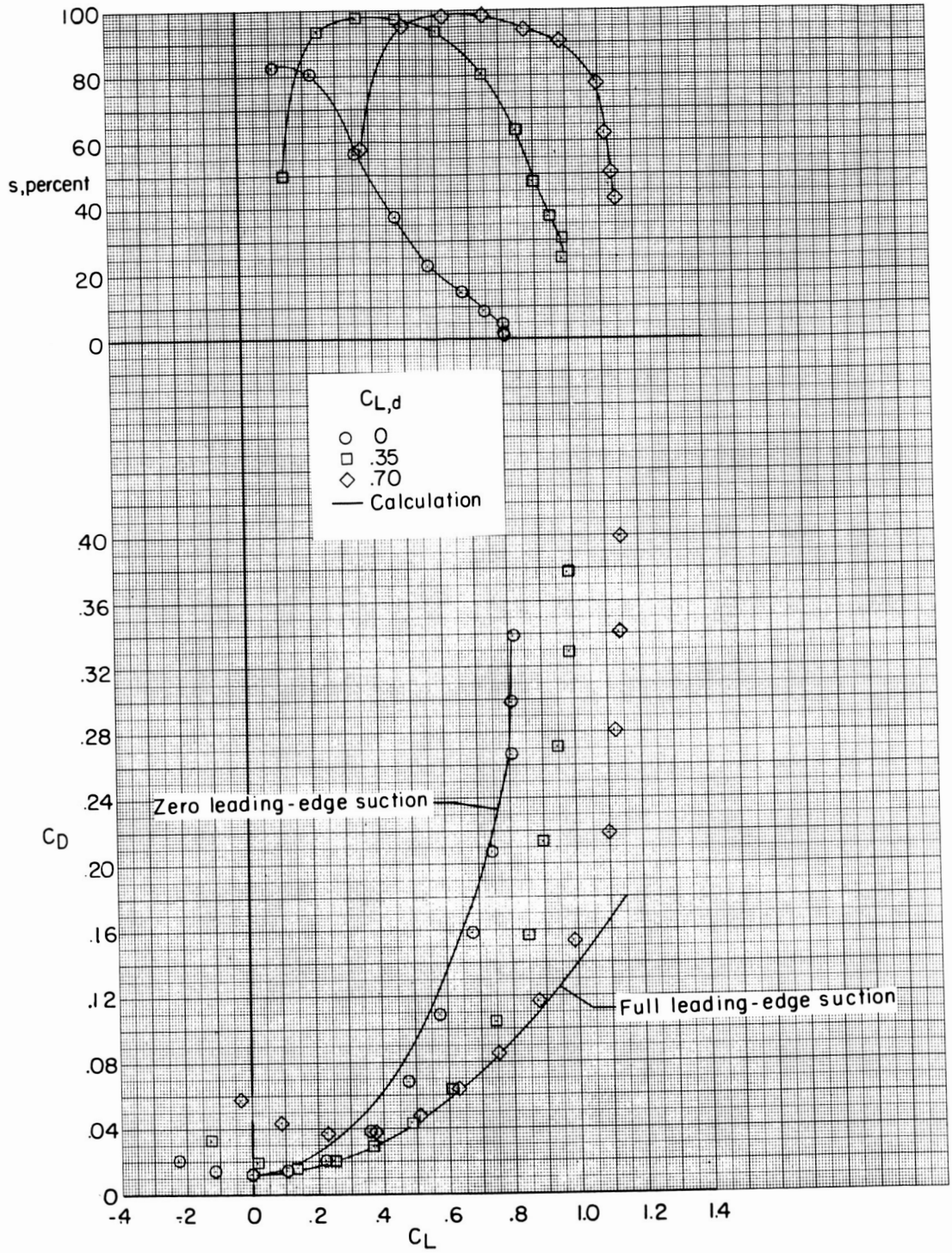

(c) M = 0.60.

Figure 5.- Continued.

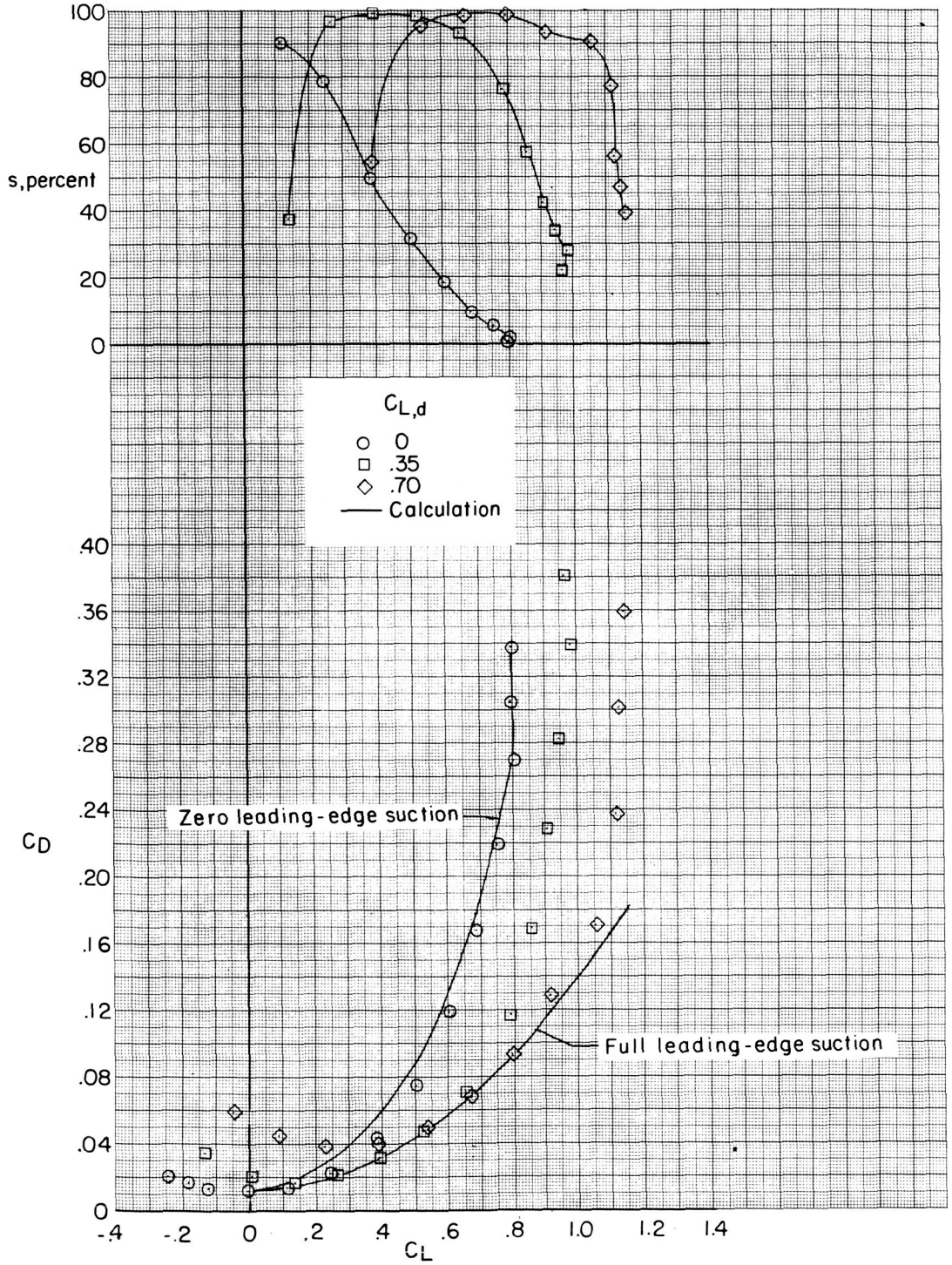

(d) M = 0.70.

Figure 5.- Concluded.

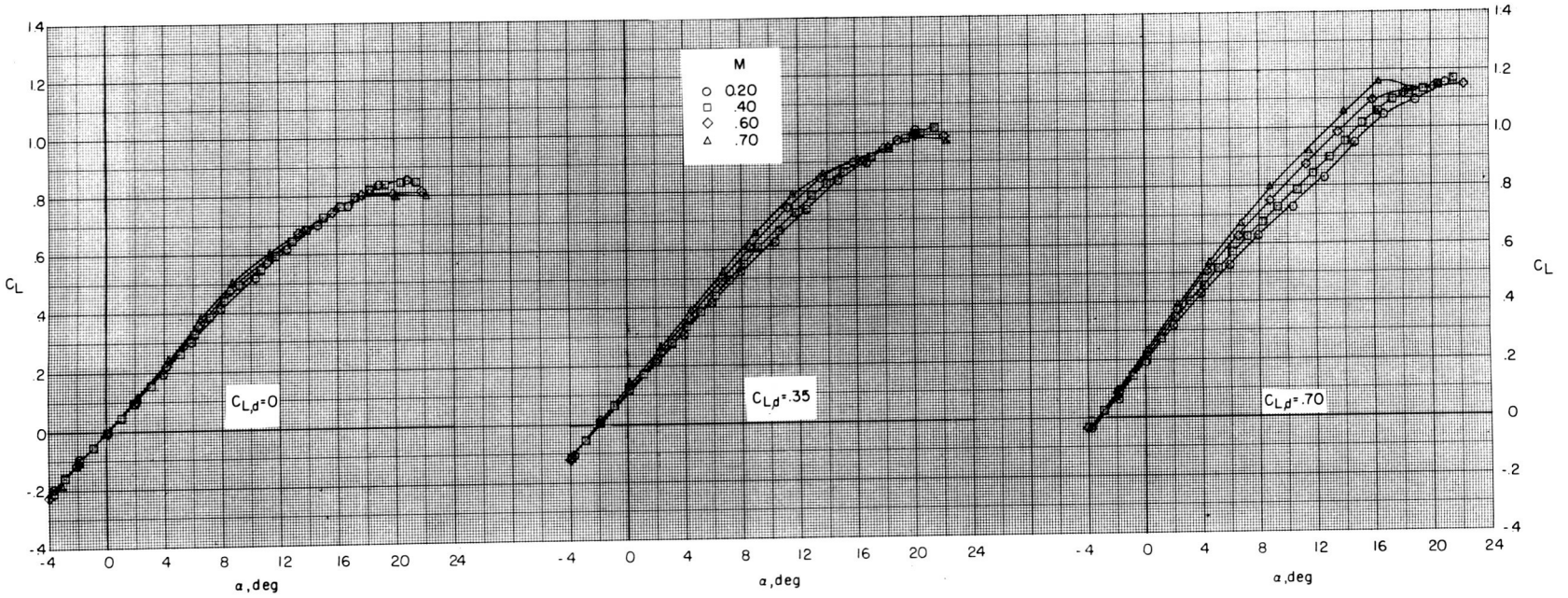

(a) C_L plotted against α.

Figure 6.- Combined effect of Mach number and Reynolds number on aerodynamic characteristics of model with short fuselage forebody and wing strake off.

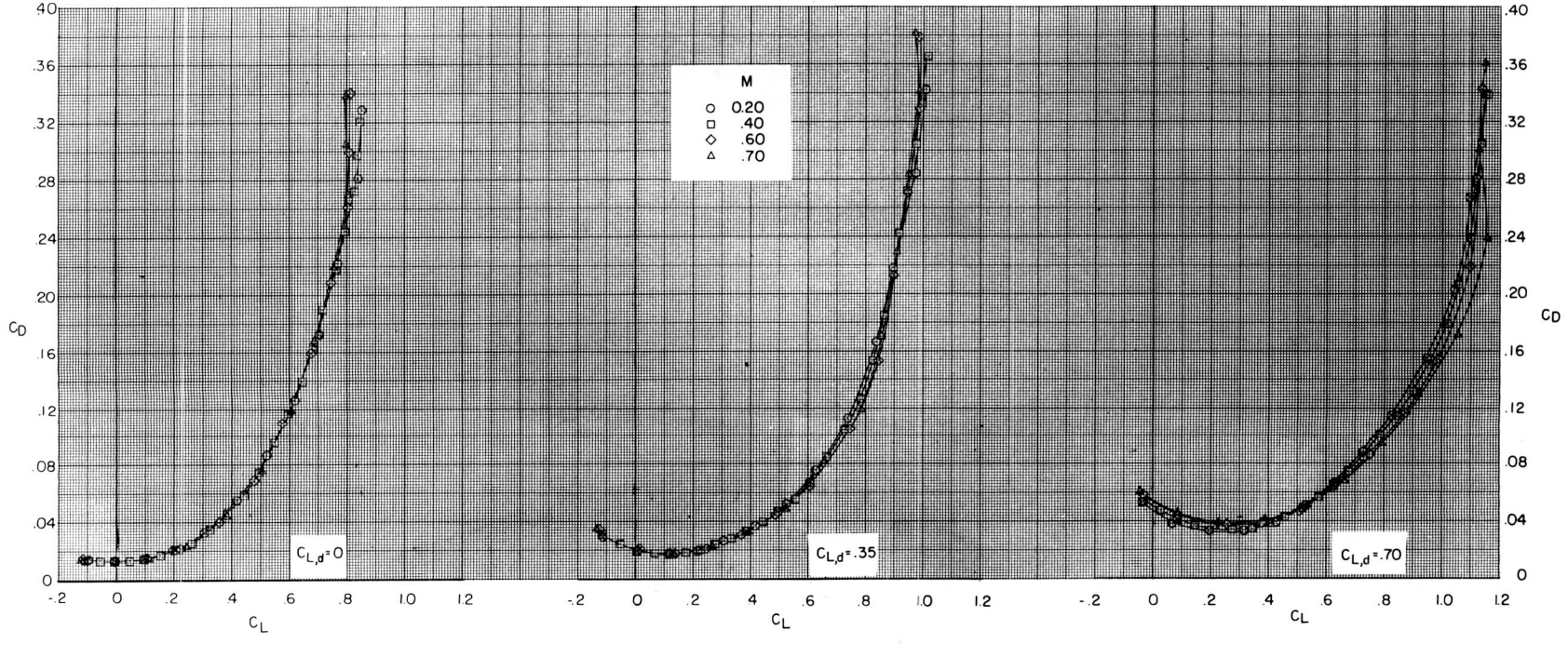

(b) C_D plotted against C_L.

Figure 6.- Continued.

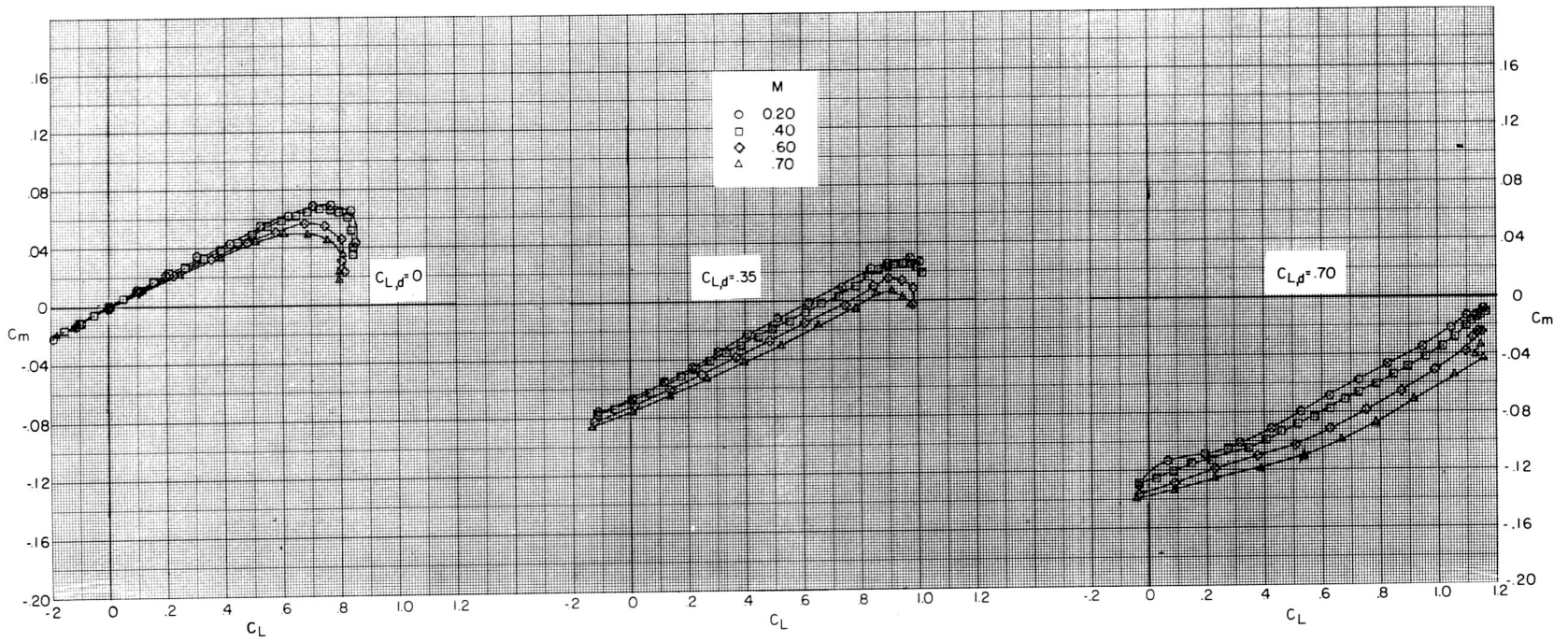

(c) C_m plotted against C_L.

Figure 6.- Concluded.

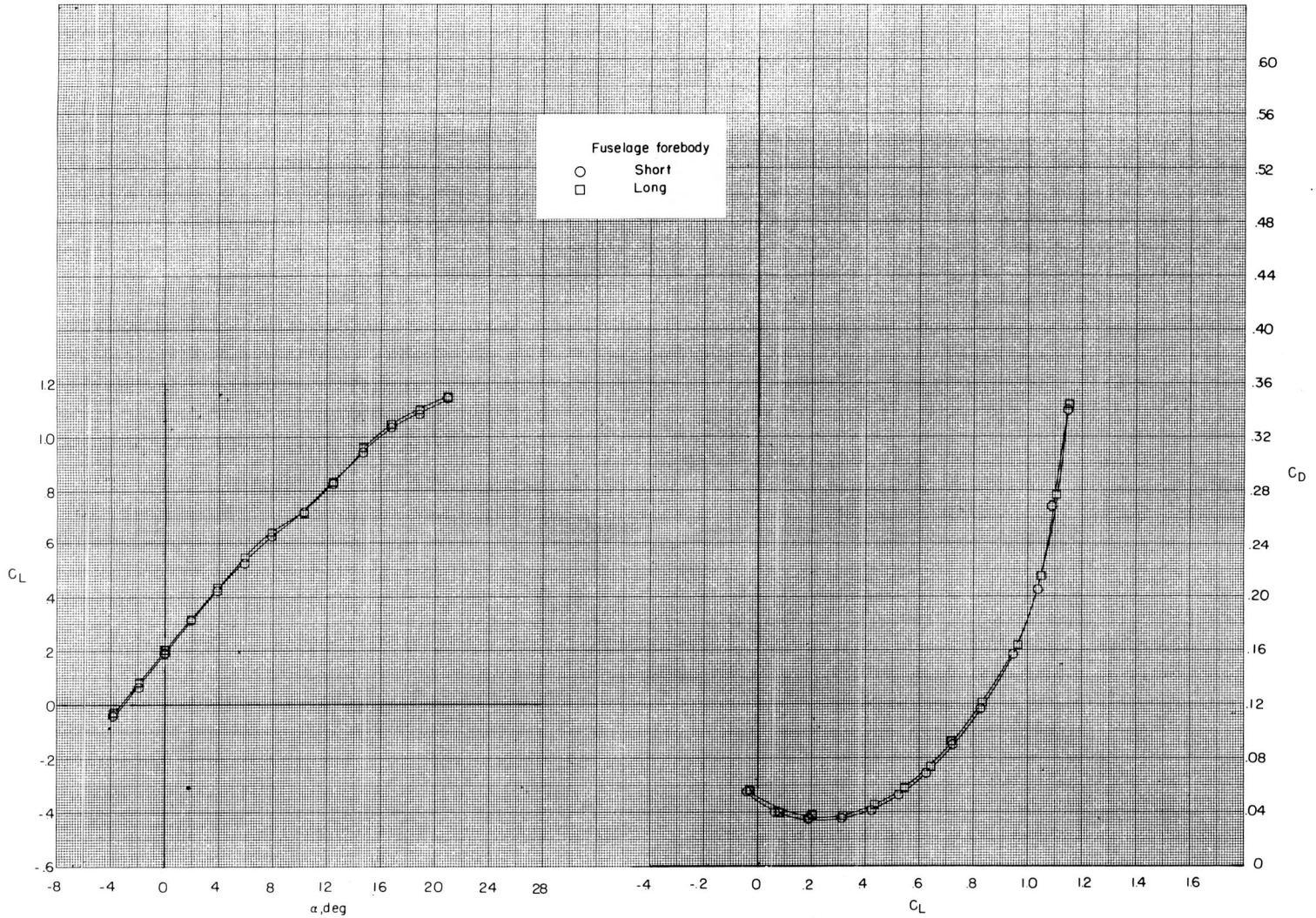

(a) M = 0.20.

Figure 7.- Effect of fuselage forebody length on aerodynamic characteristics of model with wing strake off. $C_{L,d} = 0.70$.

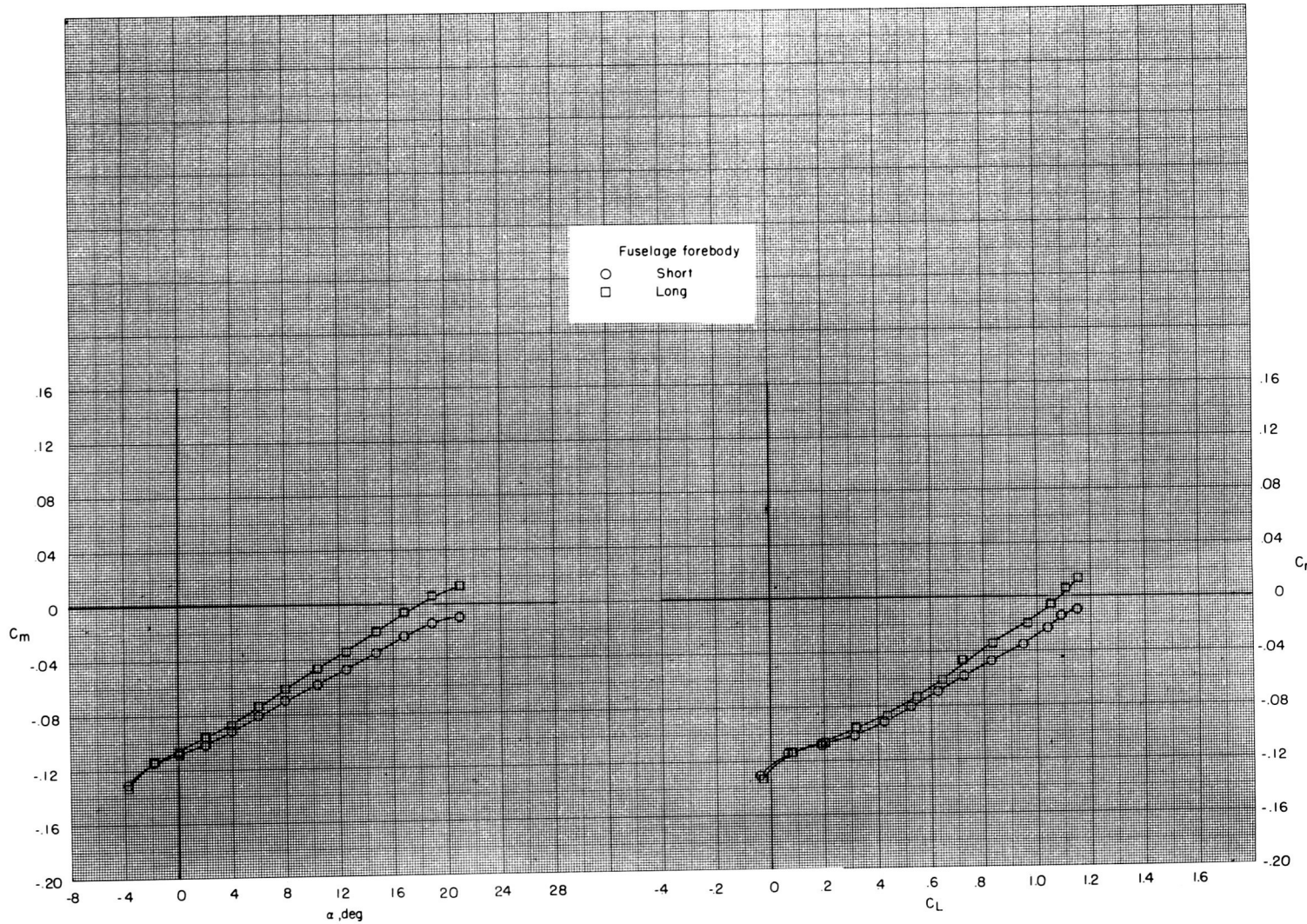

(a) Concluded.

Figure 7.- Continued.

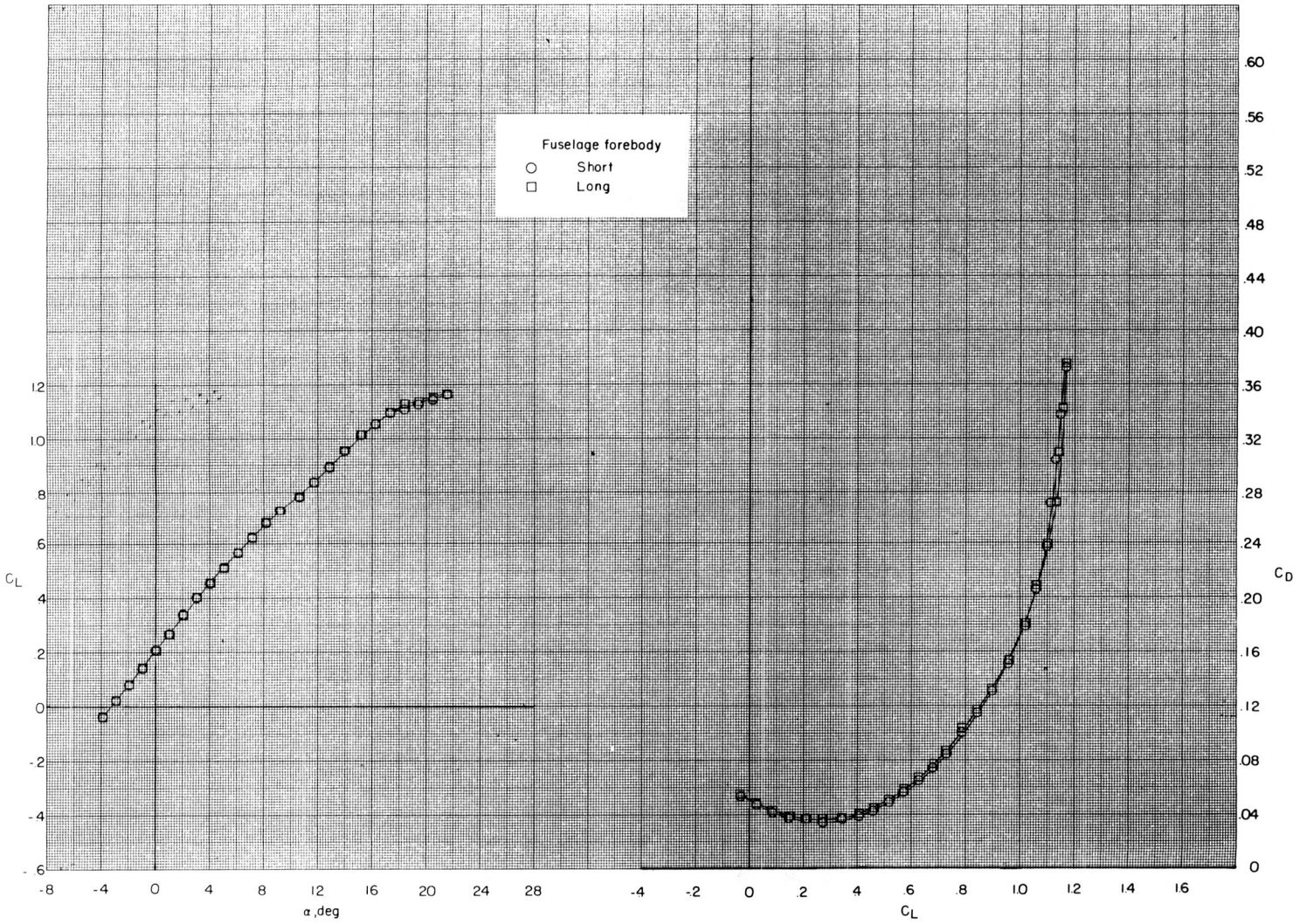

(b) M = 0.40.

Figure 7.- Continued.

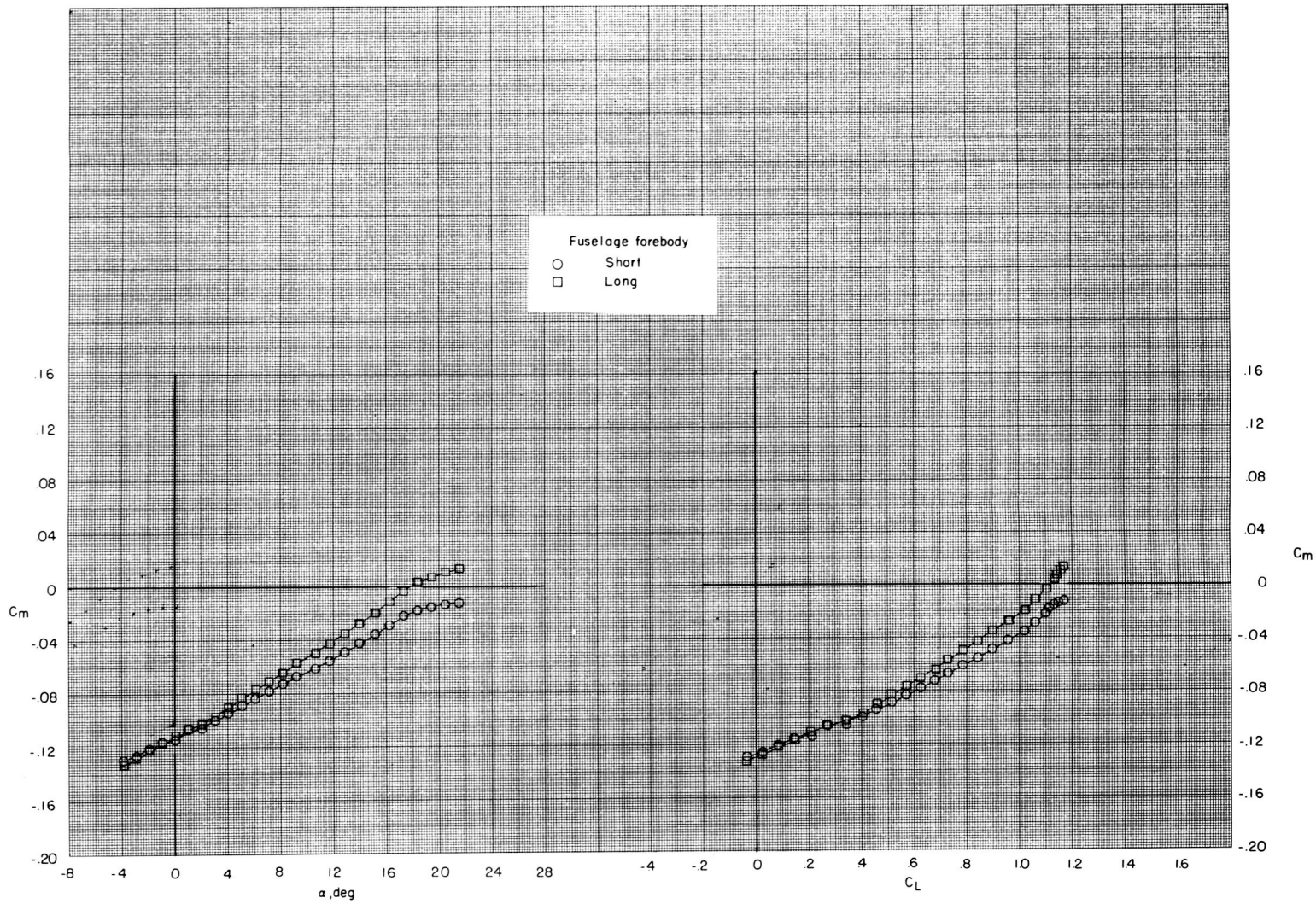

(b) Concluded.

Figure 7.- Continued.

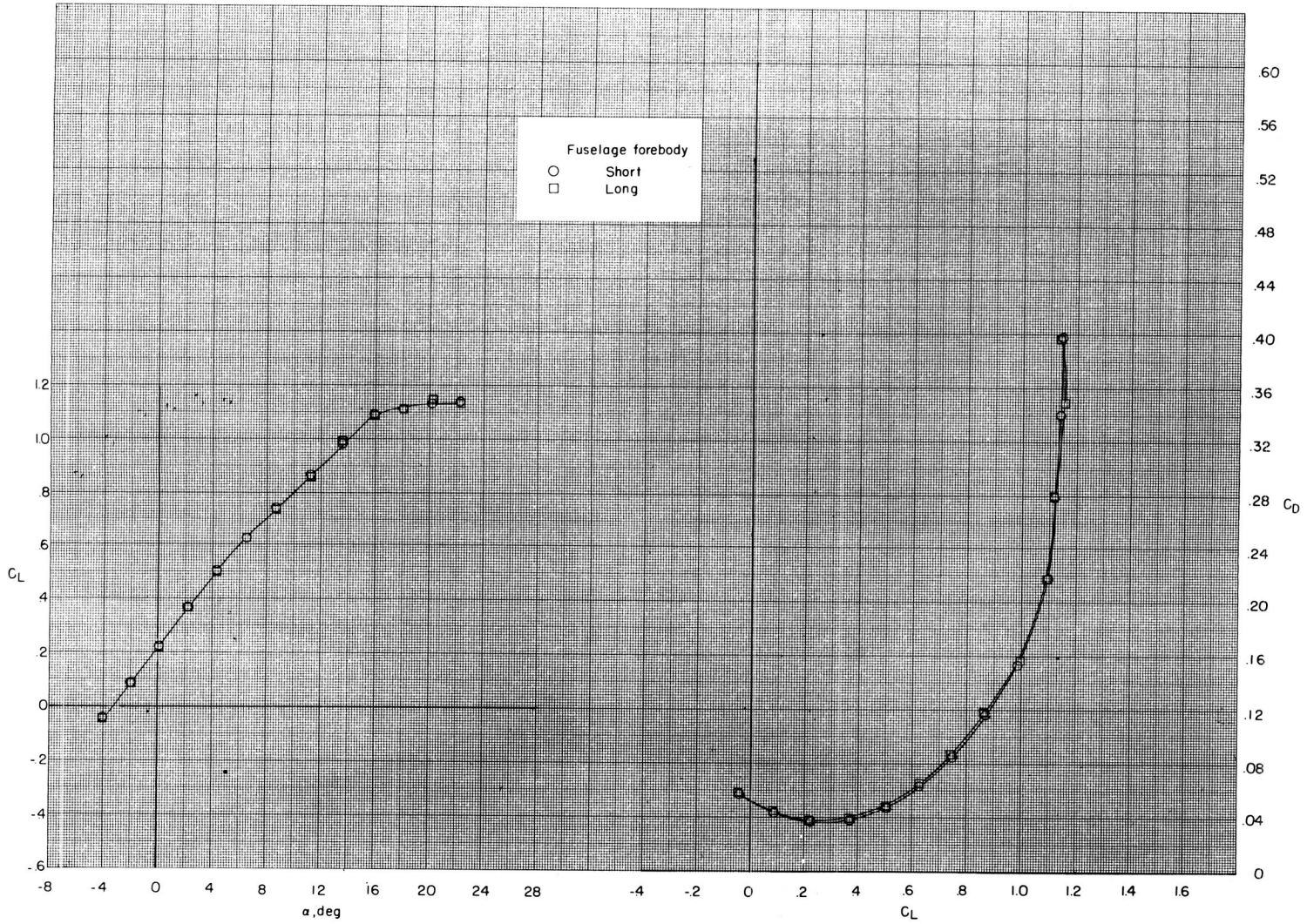

(c) M = 0.60.

Figure 7.- Continued.

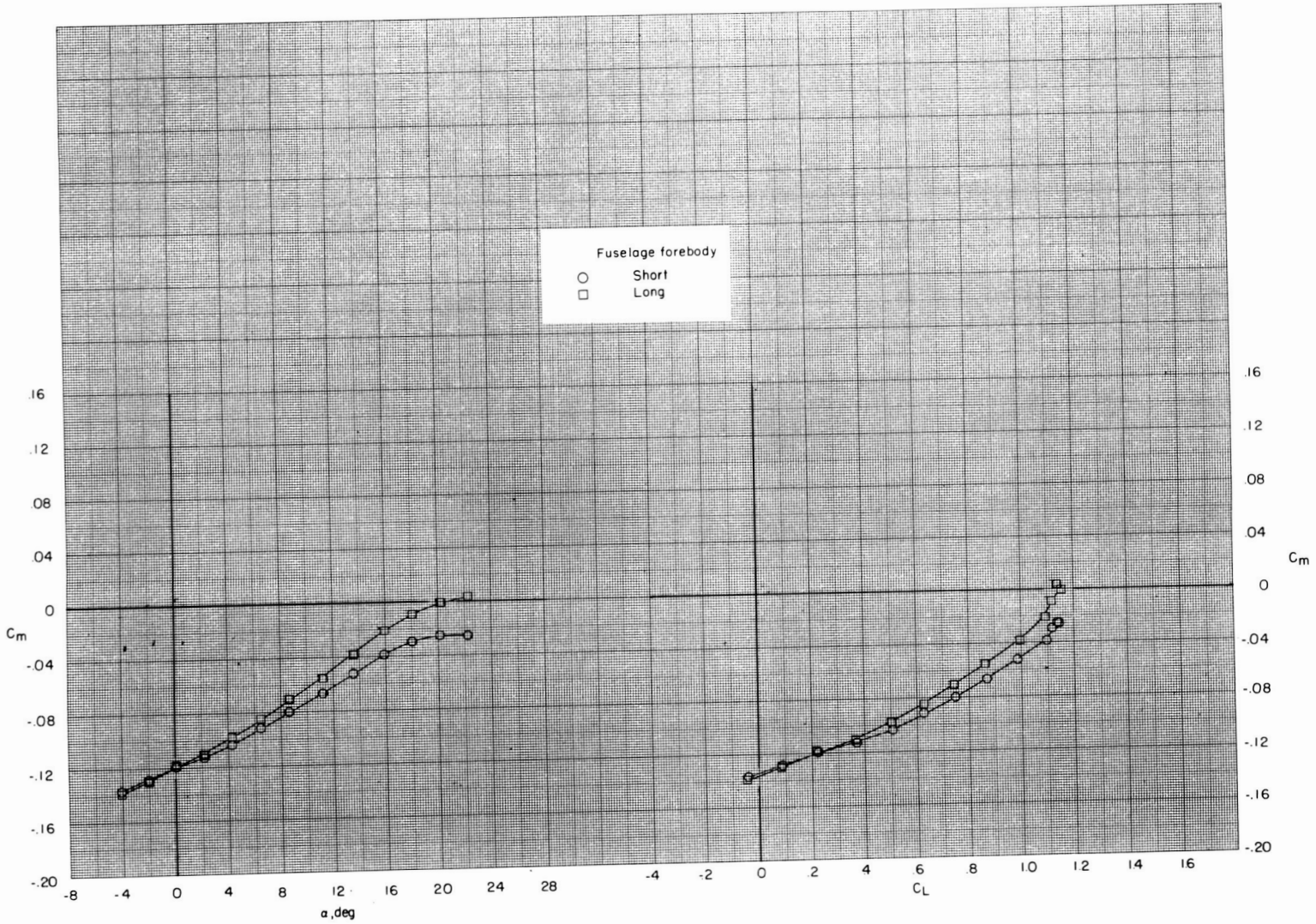

(c) Concluded.

Figure 7.- Continued.

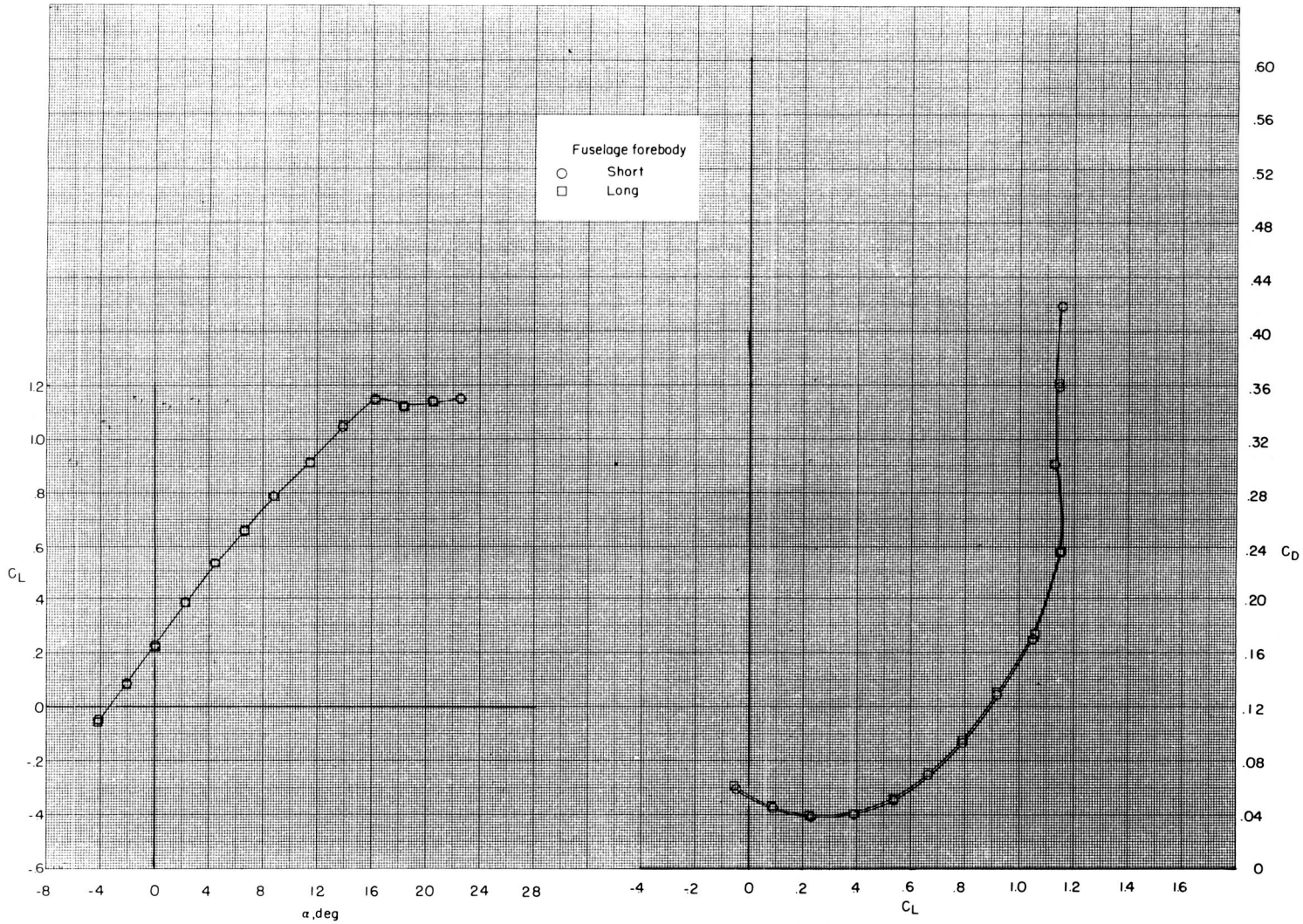

(d) M = 0.70.

Figure 7.- Continued.

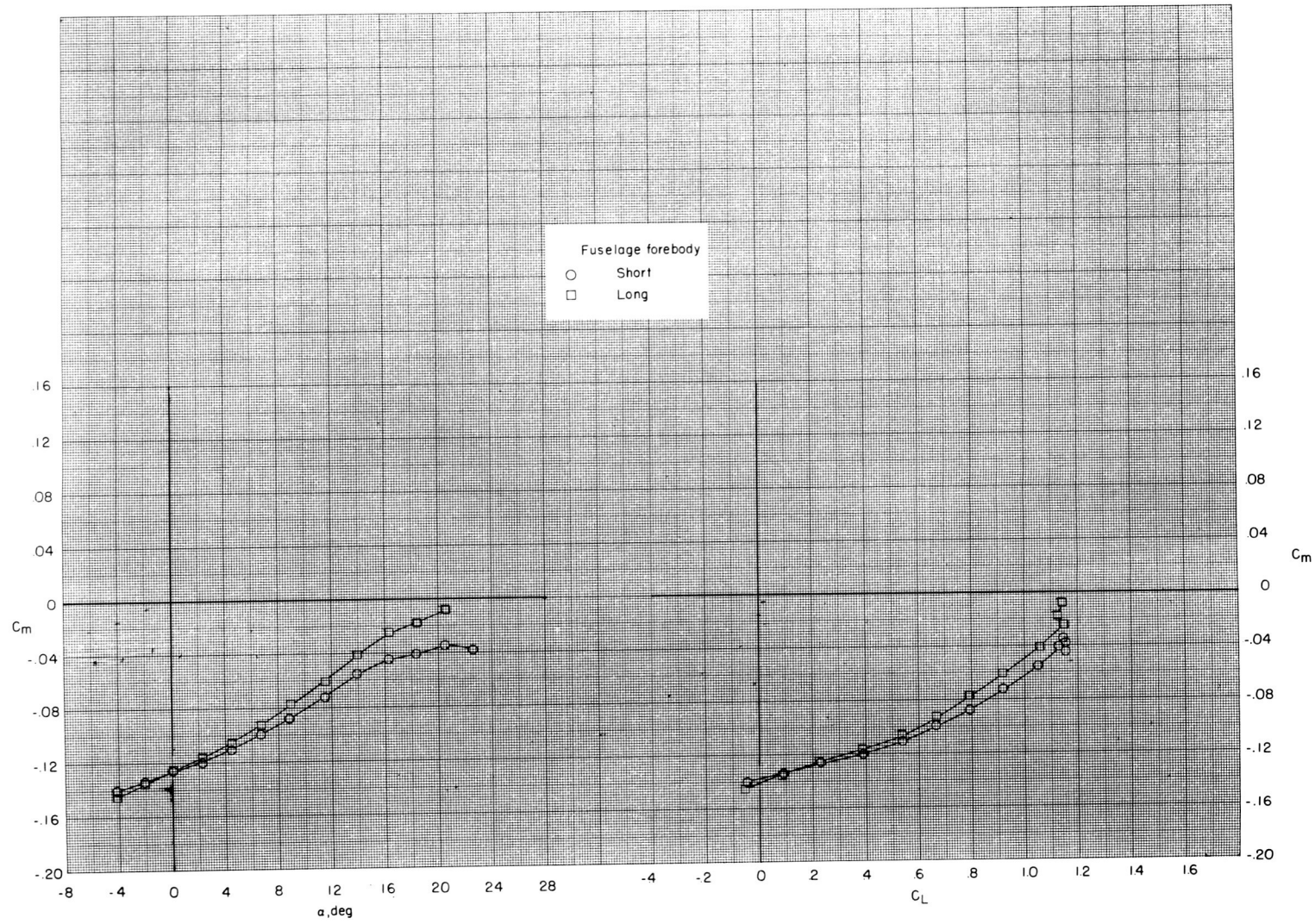

(d) Concluded.

Figure 7.- Concluded.

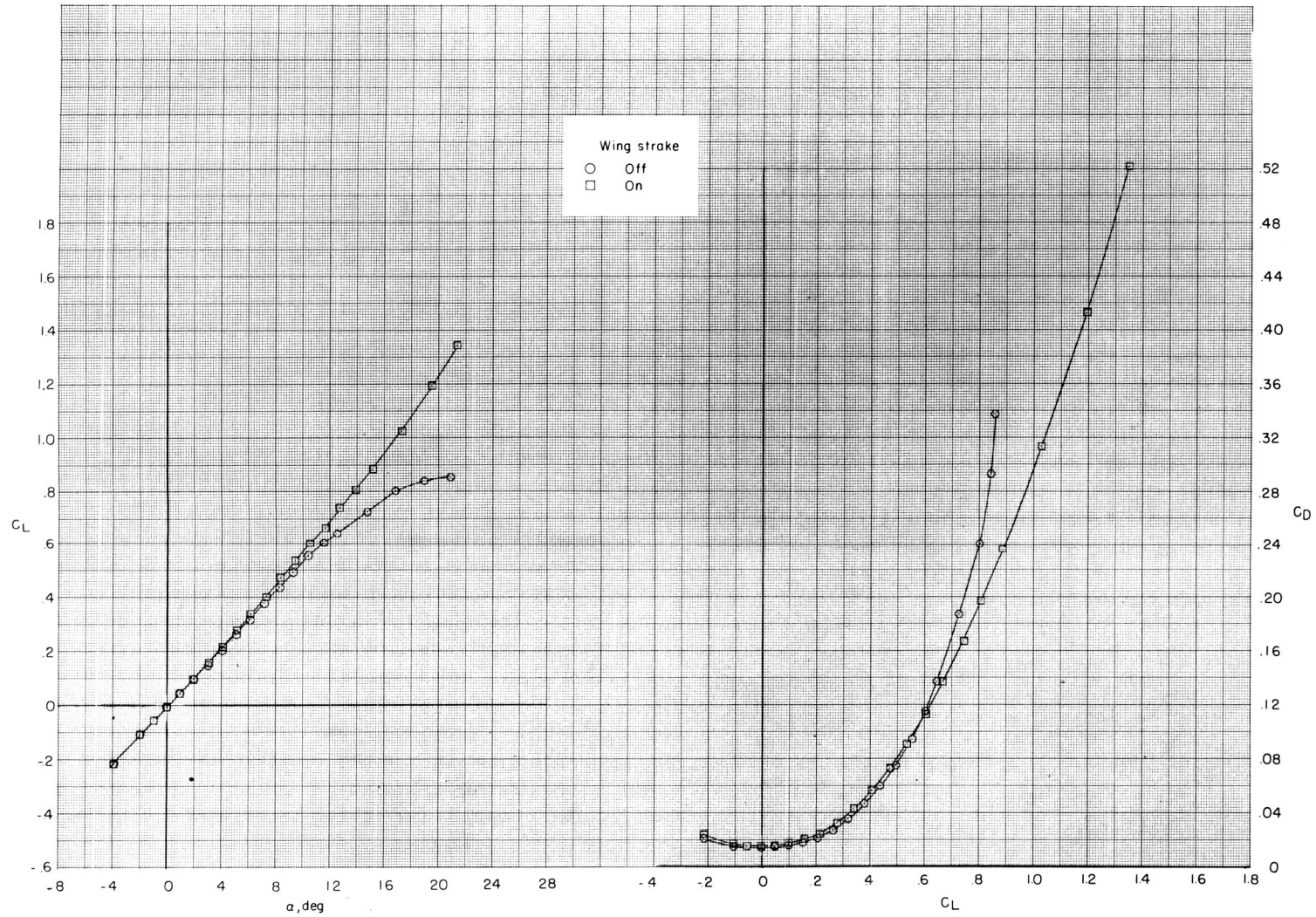

Figure 8.- Effect of wing strake on aerodynamic characteristics of model with long fuselage forebody. $C_{L,d} = 0$; $M = 0.40$.

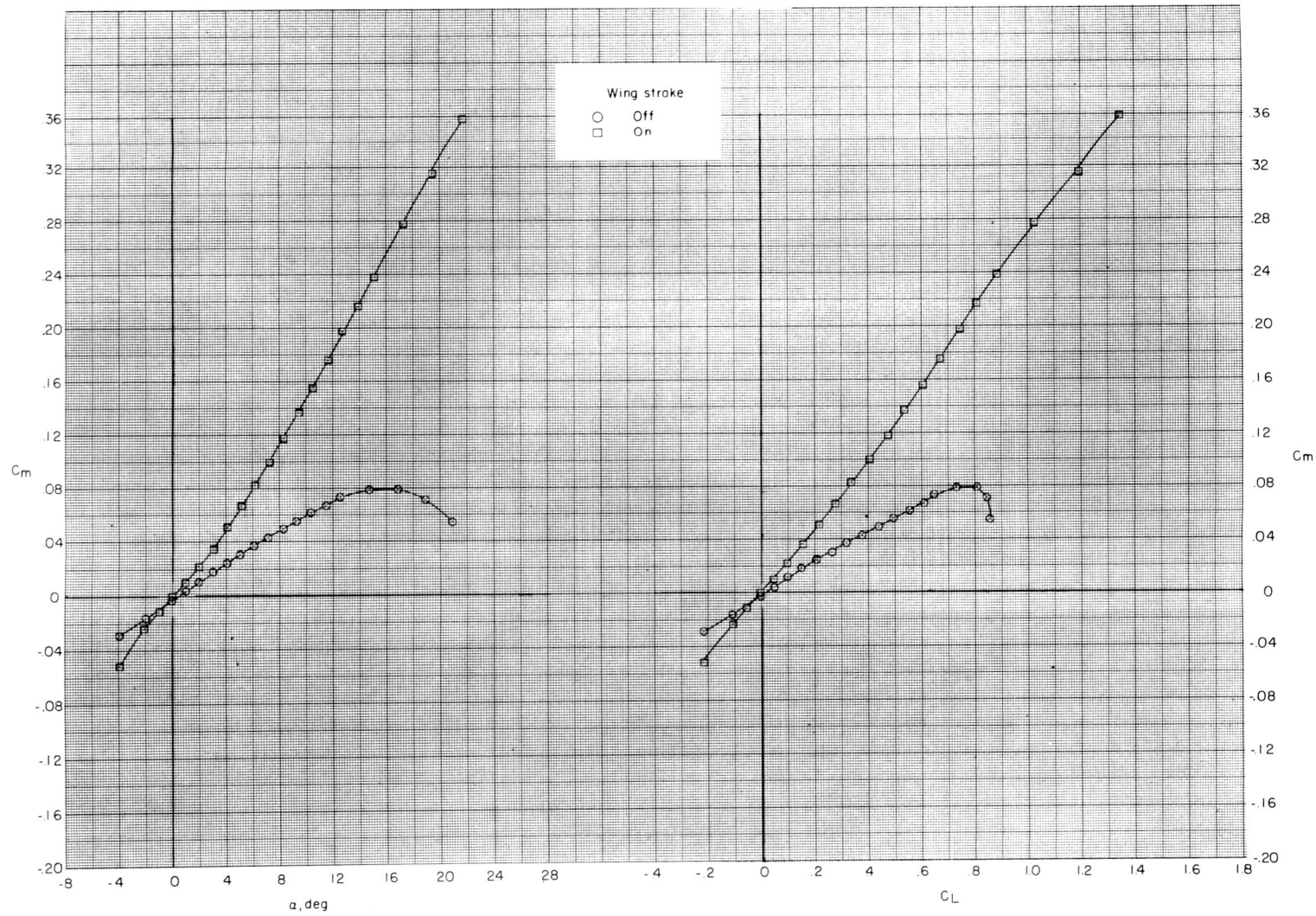

Figure 8.- Concluded.

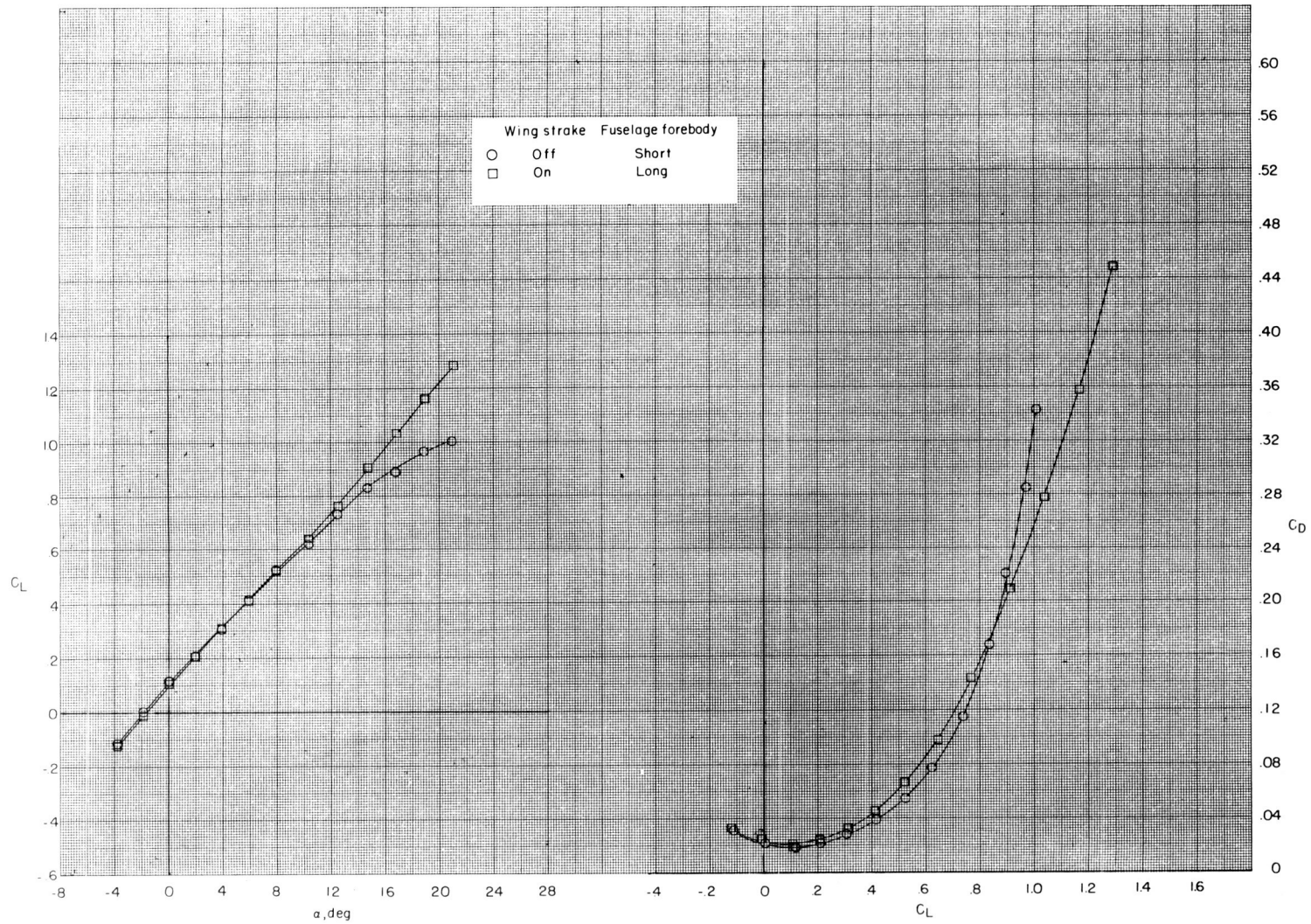

(a) M = 0.20.

Figure 9.- Effect of wing strake on aerodynamic characteristics of model. $C_{L,d} = 0.35$.

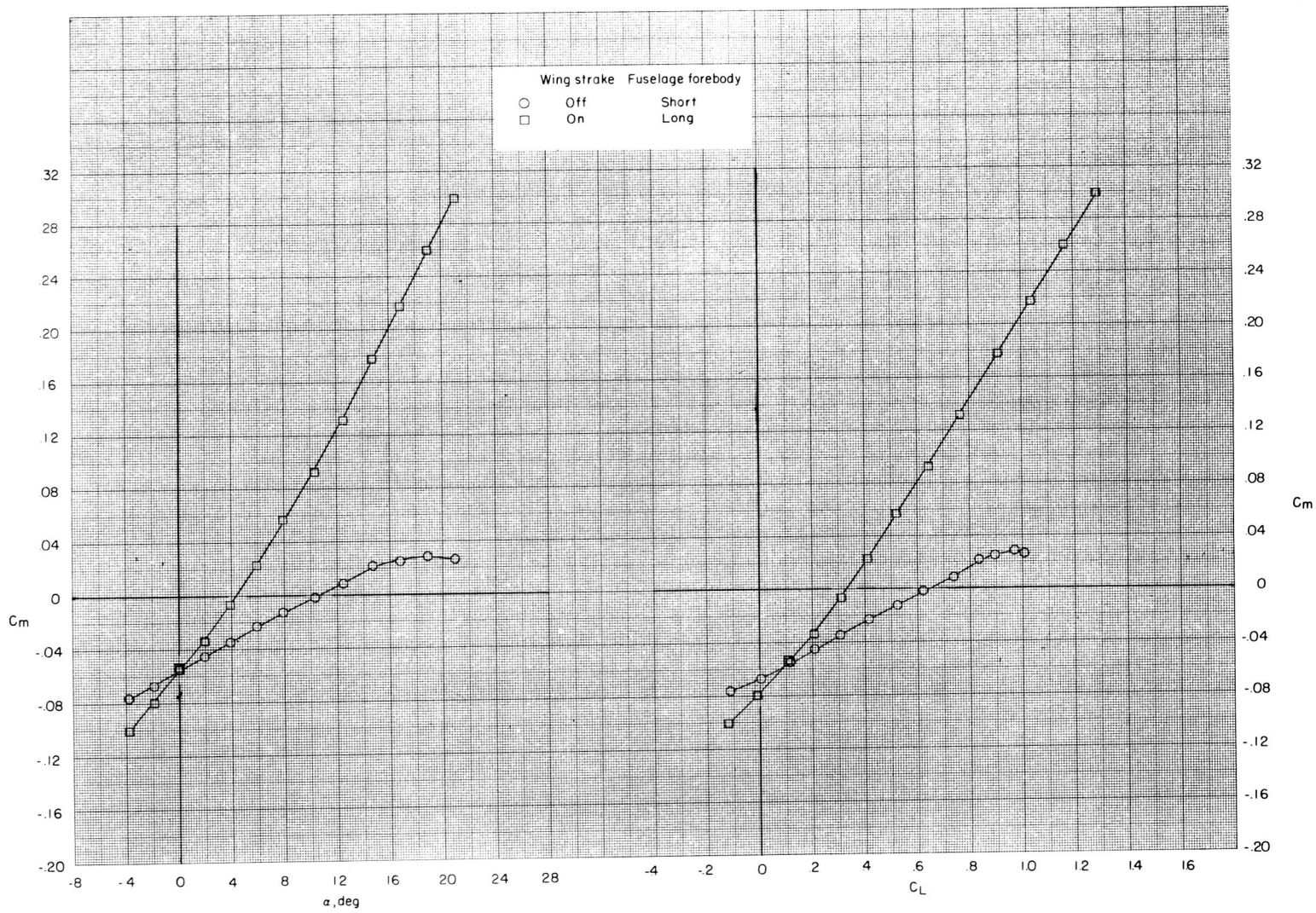

(a) Concluded.

Figure 9.- Continued.

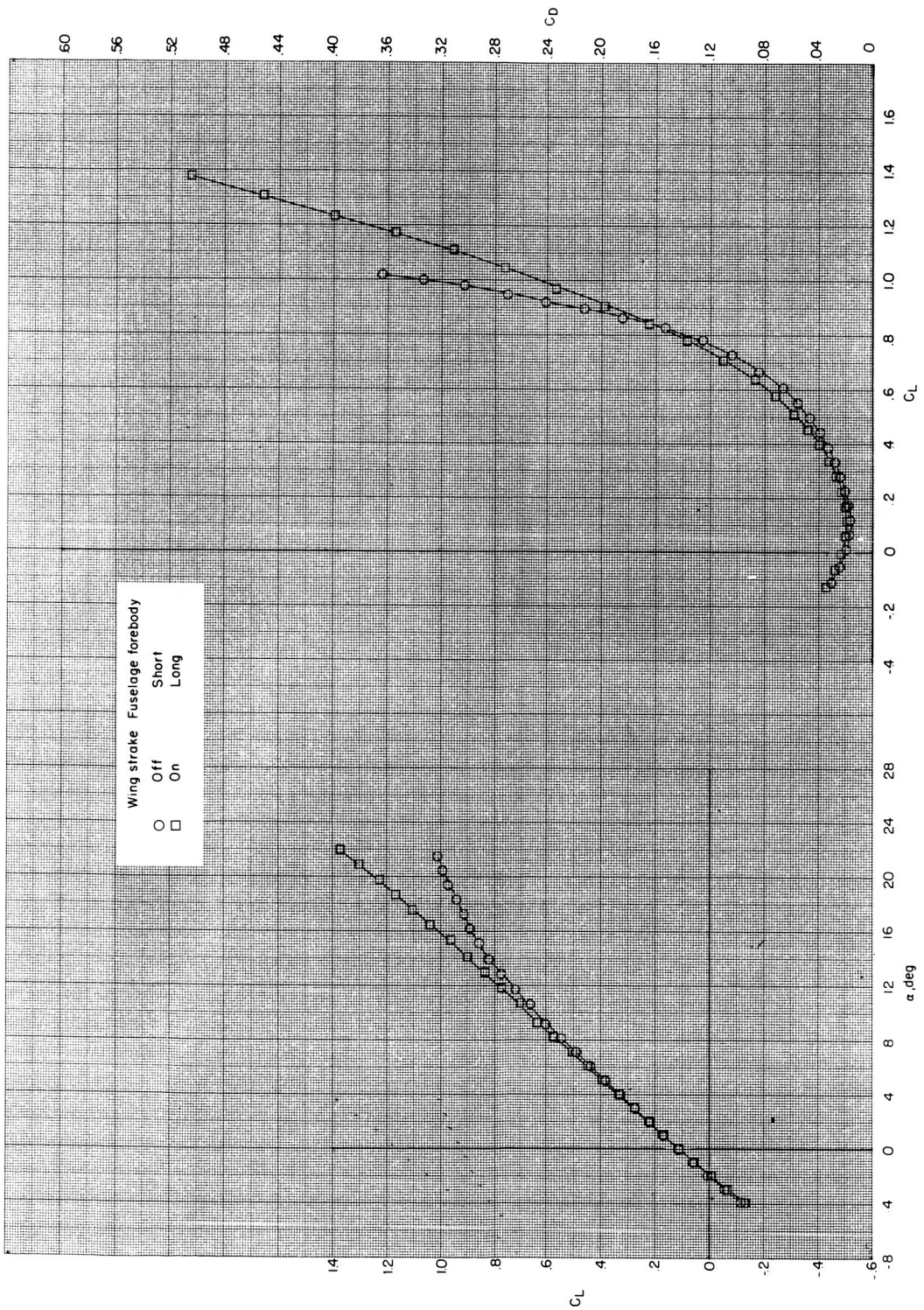

(b) M = 0.40.

Figure 9.- Continued.

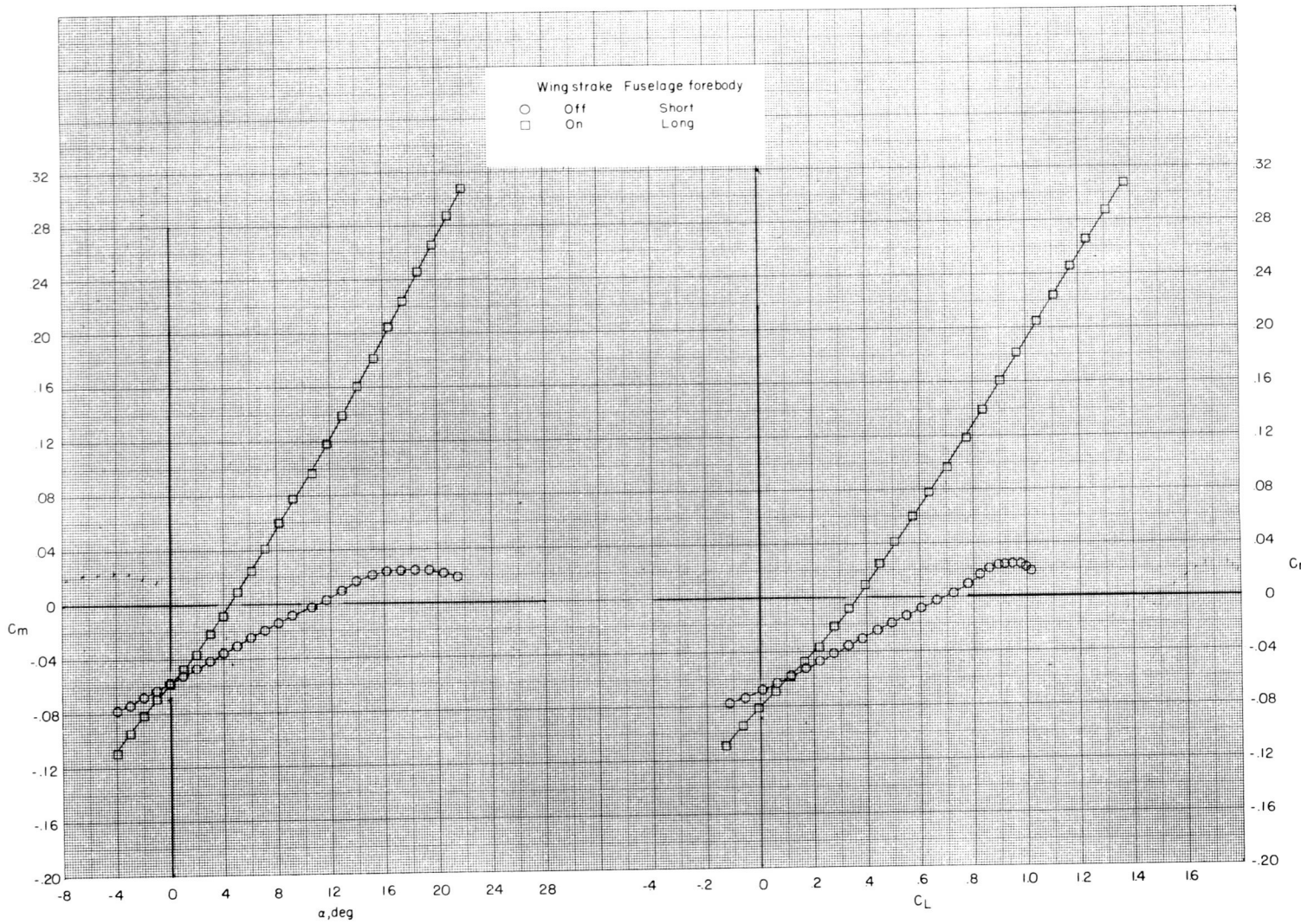

(b) Concluded.

Figure 9.- Continued.

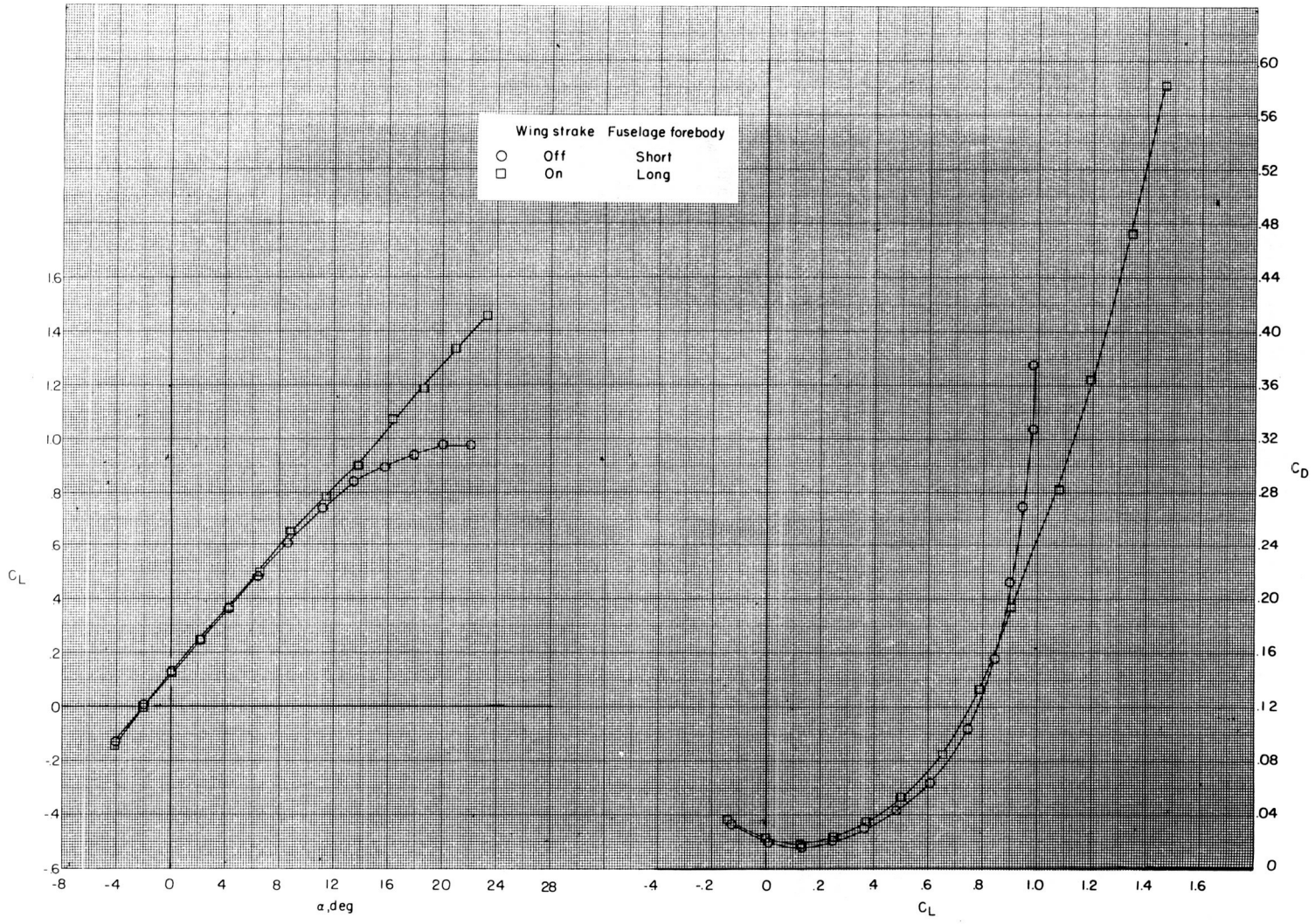

(c) M = 0.60.

Figure 9.- Continued.

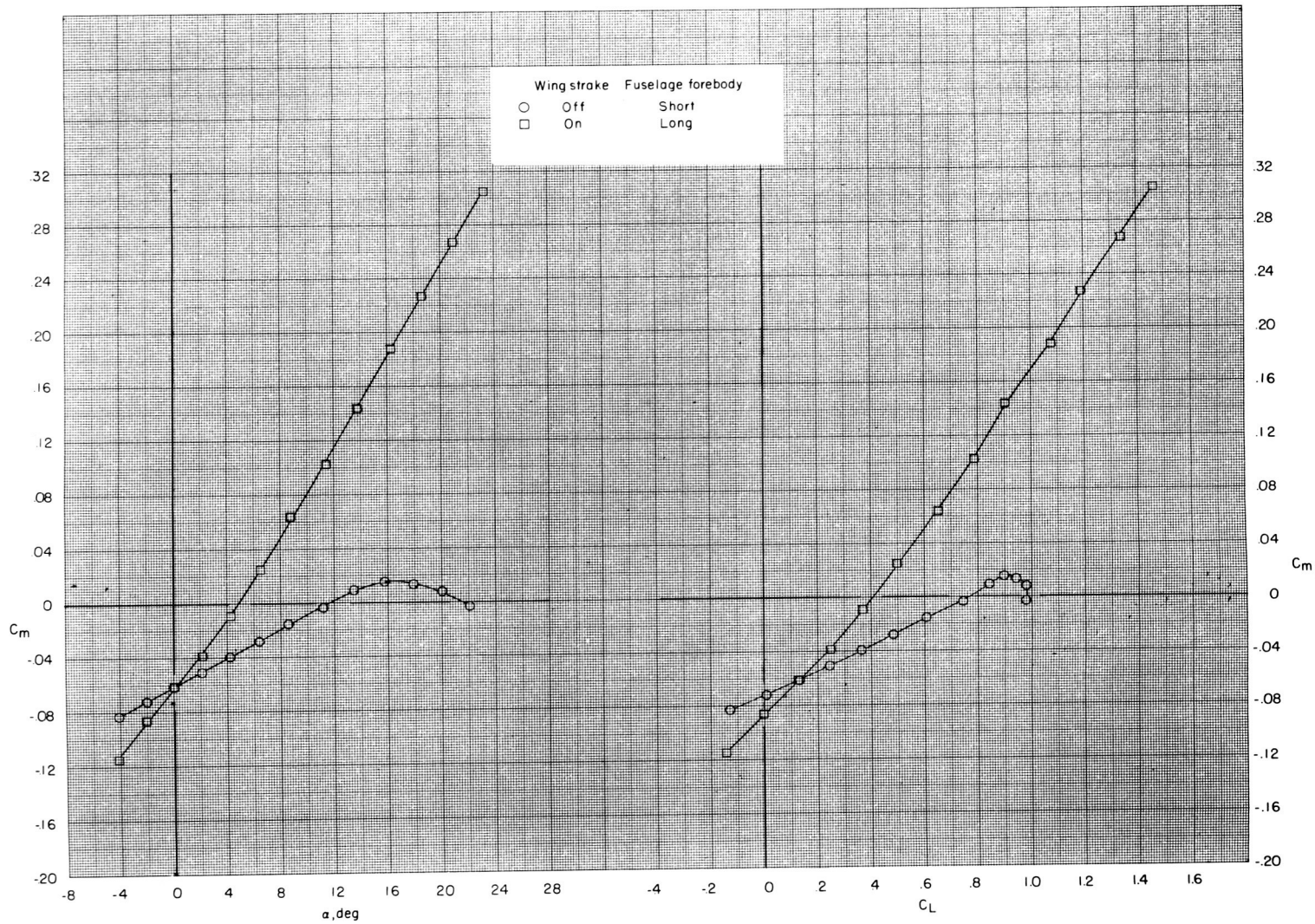

(c) Concluded.

Figure 9.- Continued.

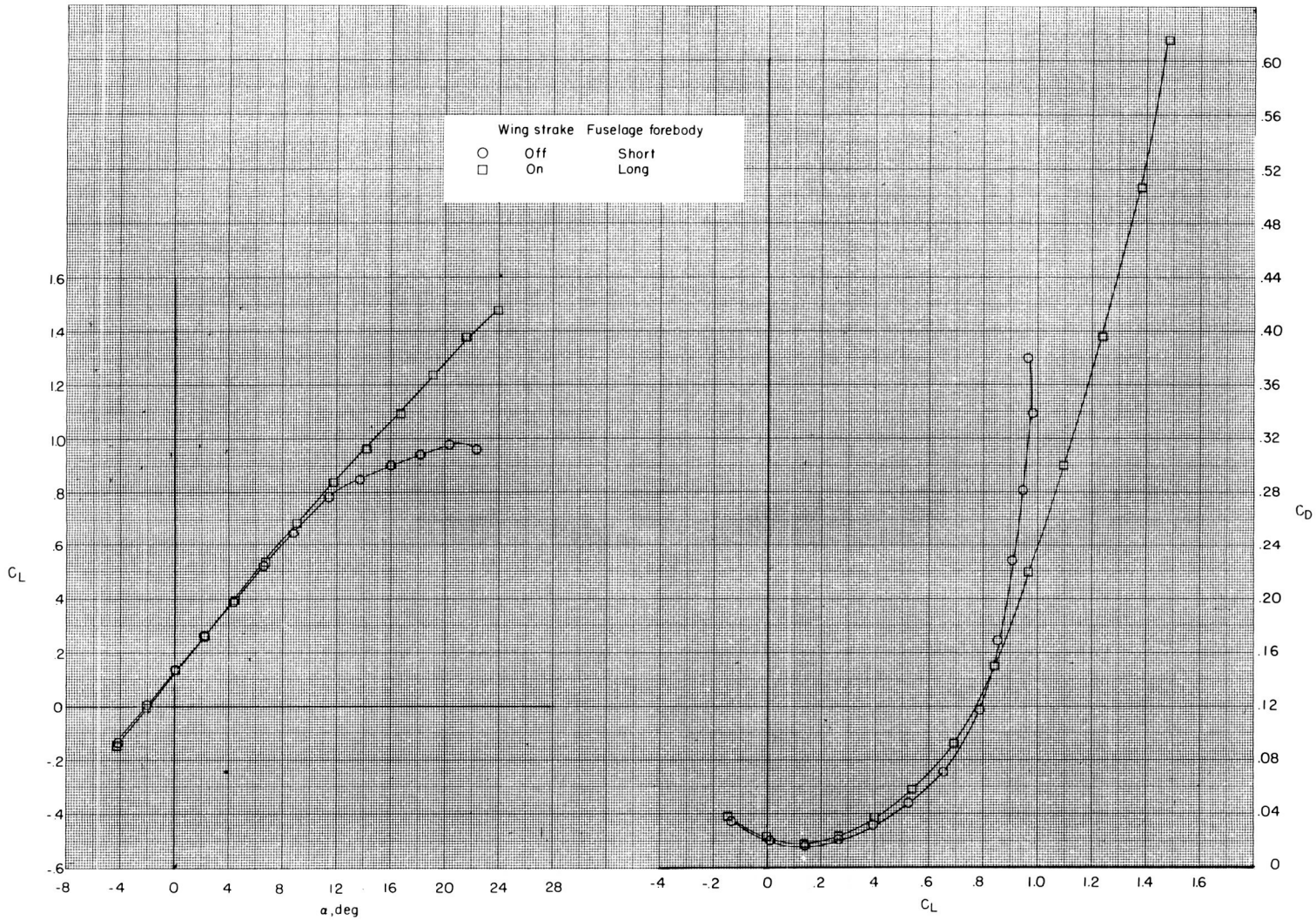

(d) M = 0.70.

Figure 9.- Continued.

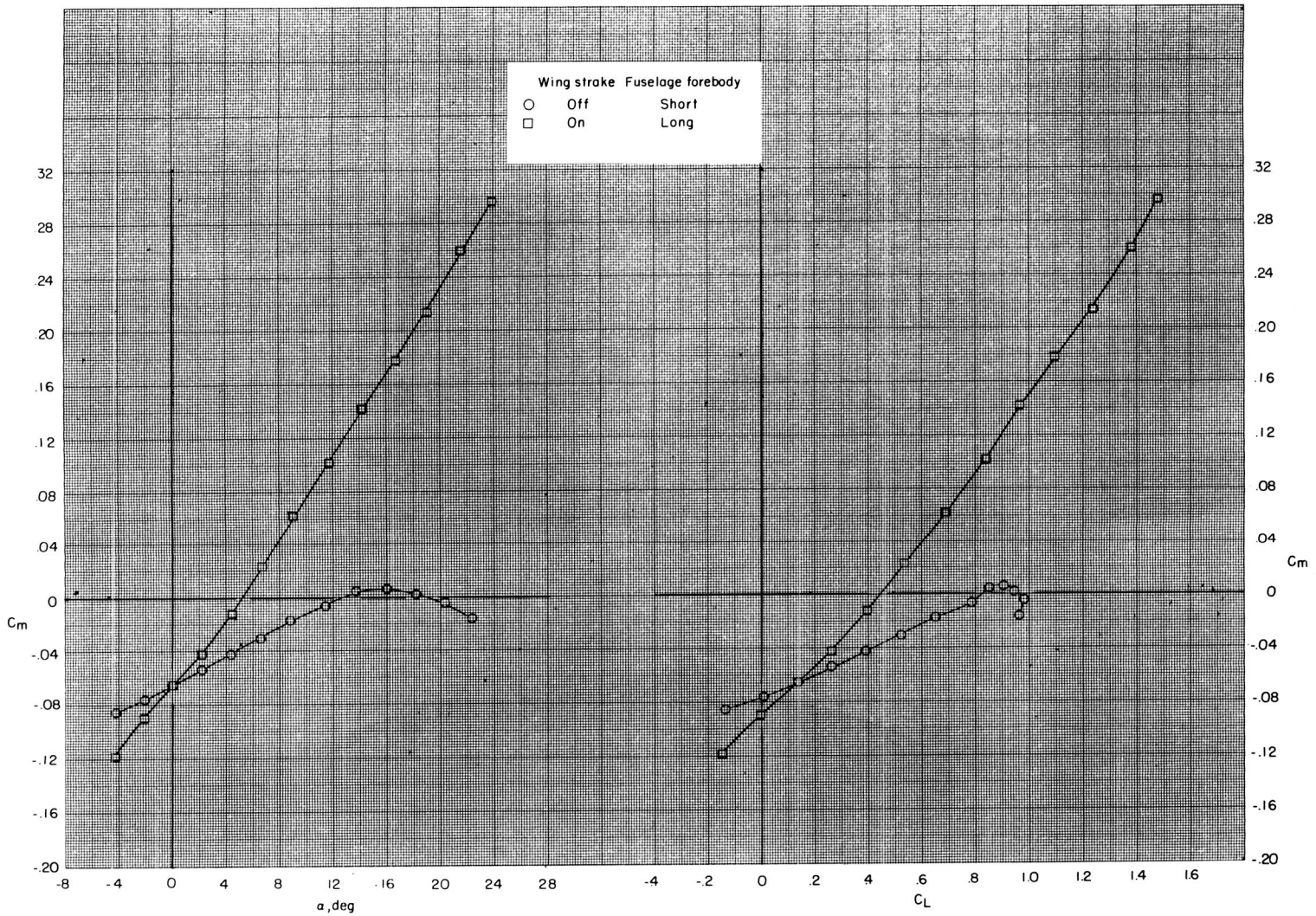

(d) Concluded.

Figure 9.- Concluded.

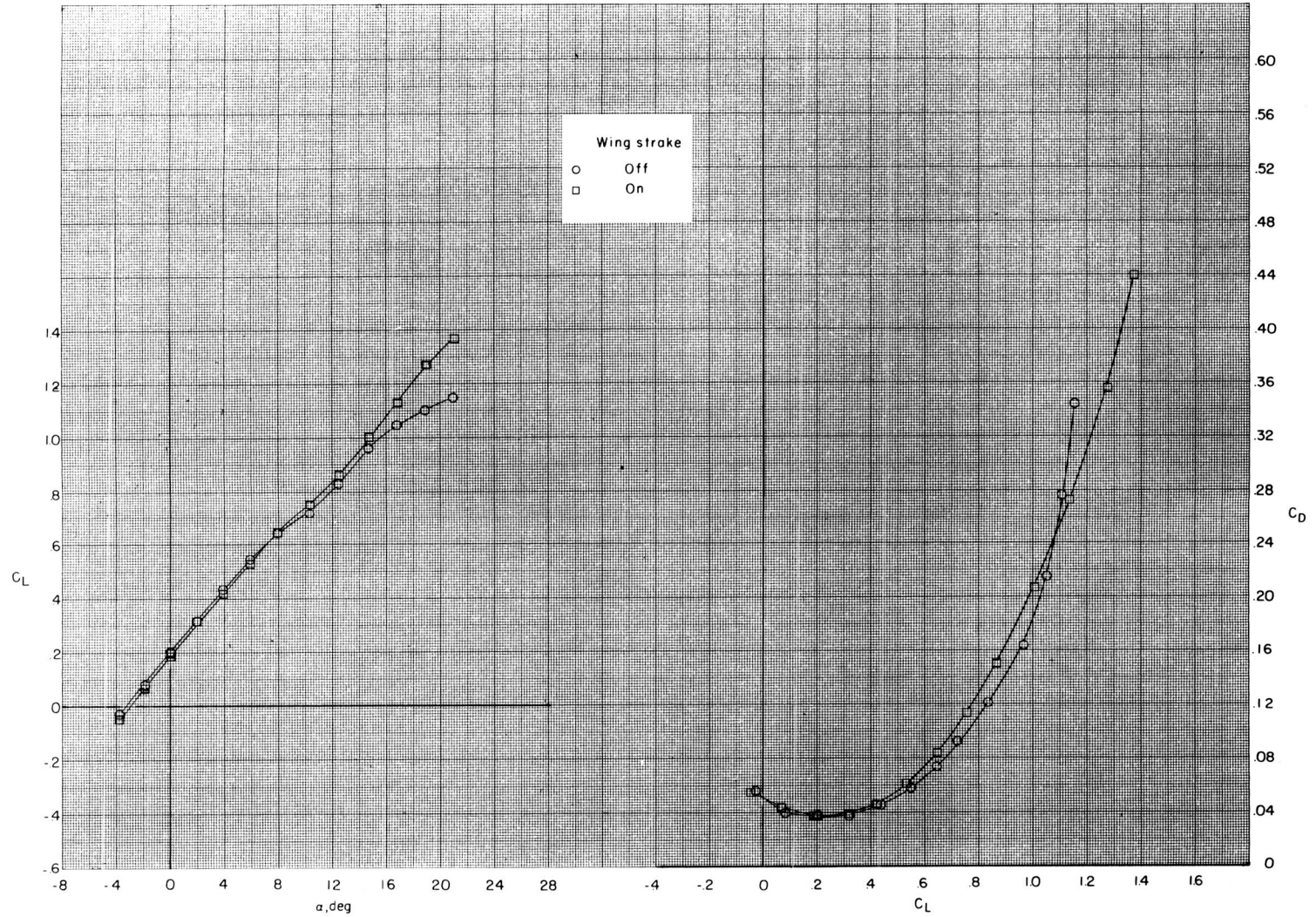

(a) M = 0.20.

Figure 10.- Effect of wing strake on aerodynamic characteristics of model with long fuselage forebody. $C_{L,d} = 0.70$.

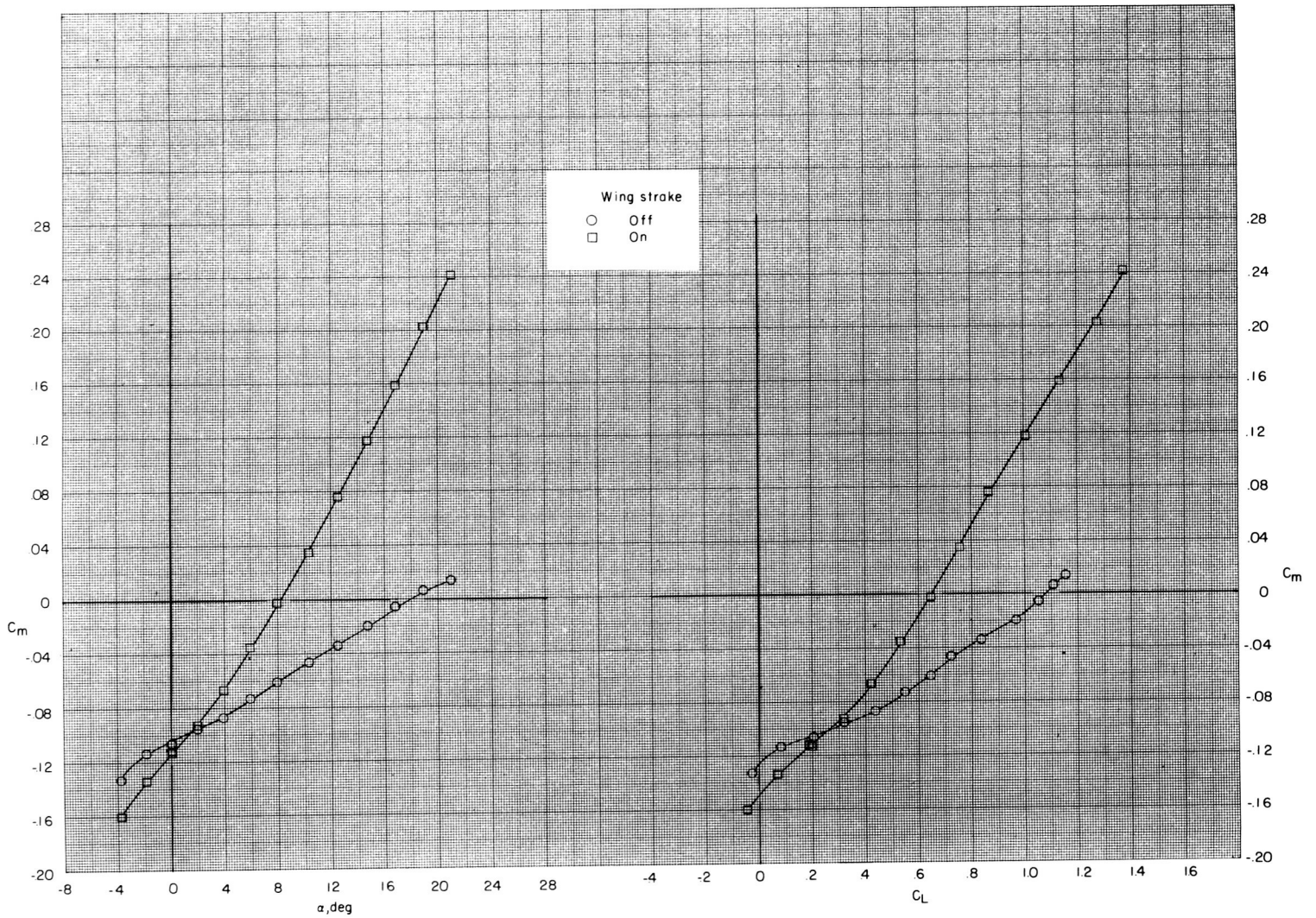

(a) Concluded.

Figure 10.- Continued.

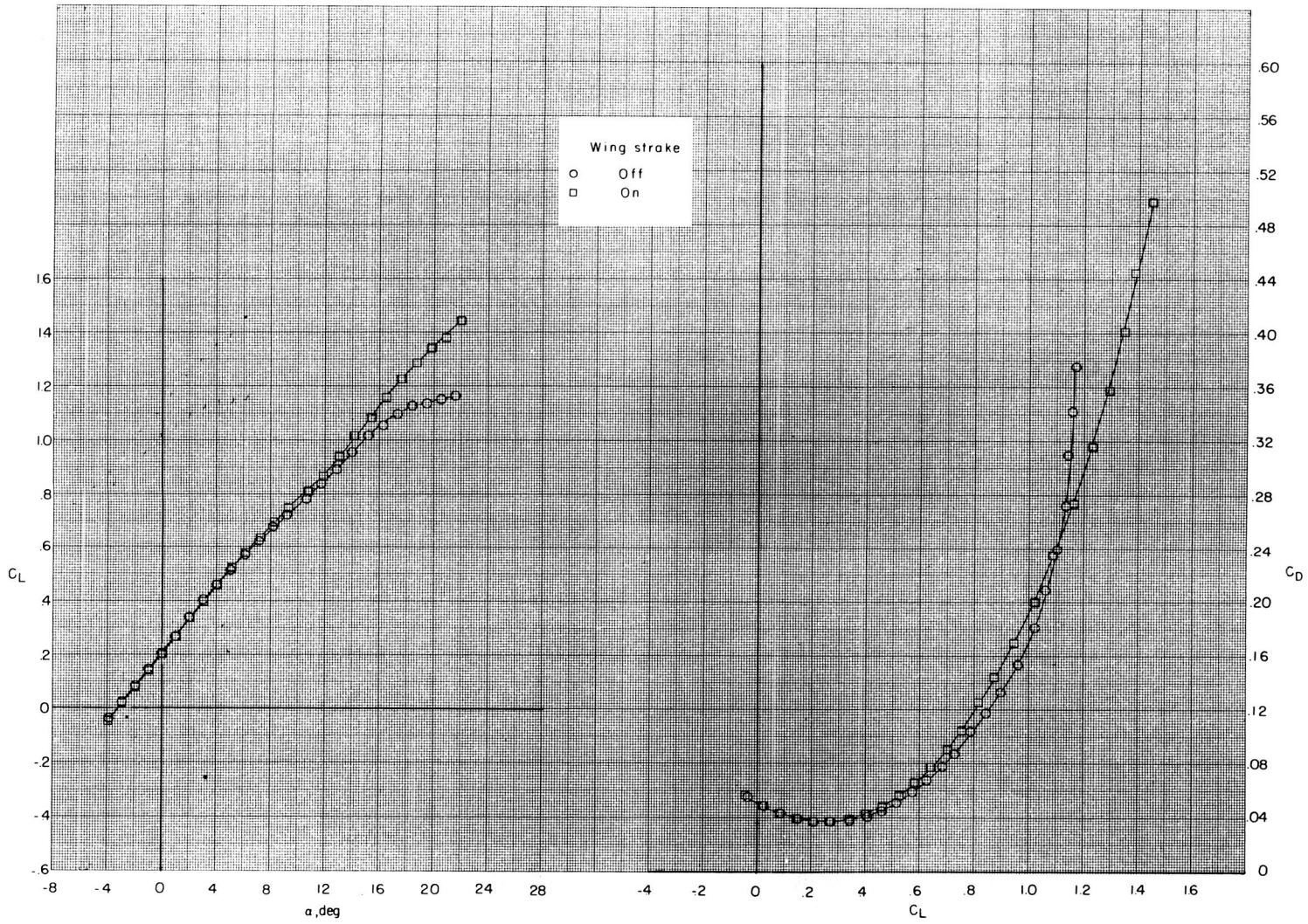

(b) M = 0.40.

Figure 10.- Continued.

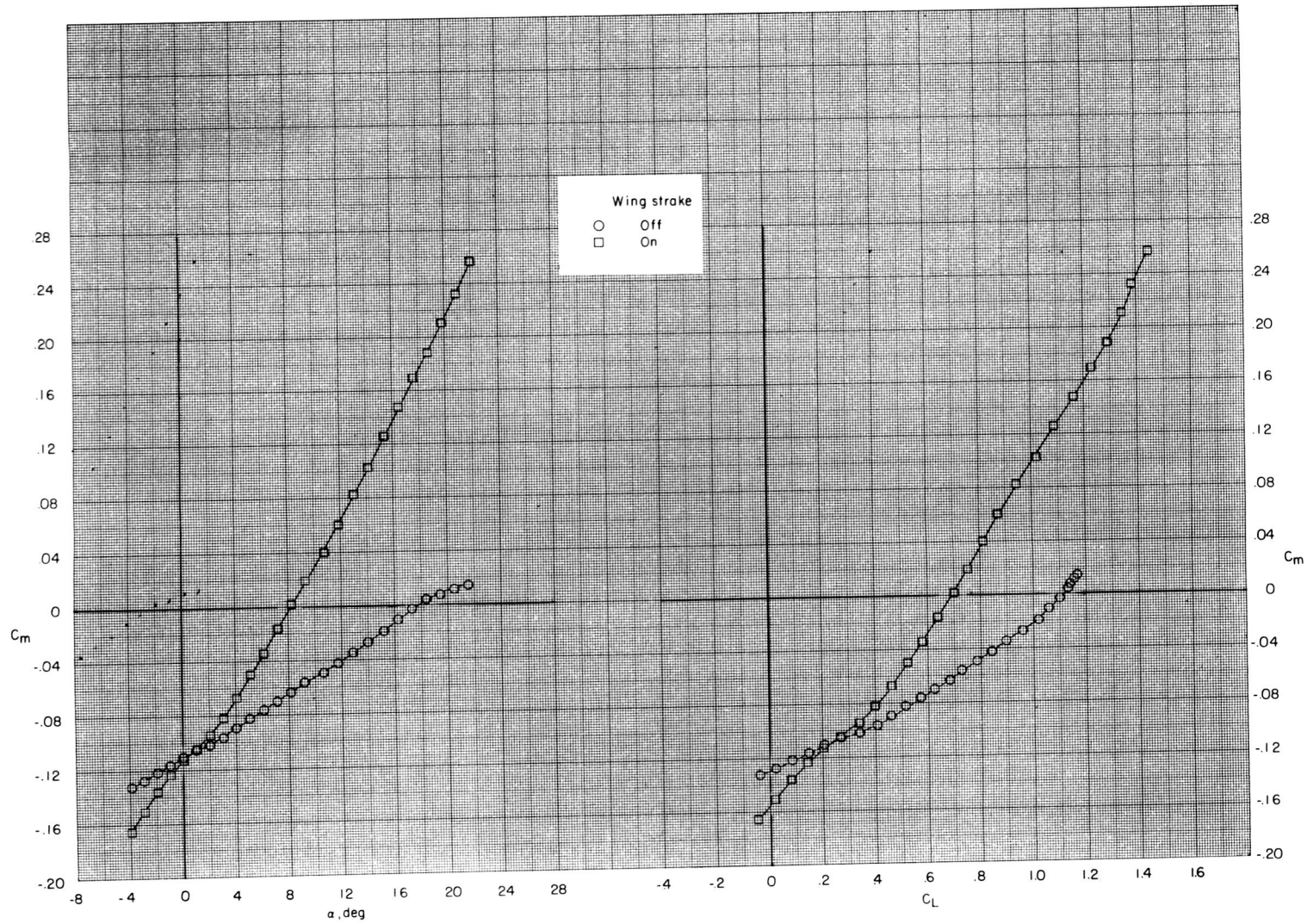

(b) Concluded.

Figure 10.- Continued.

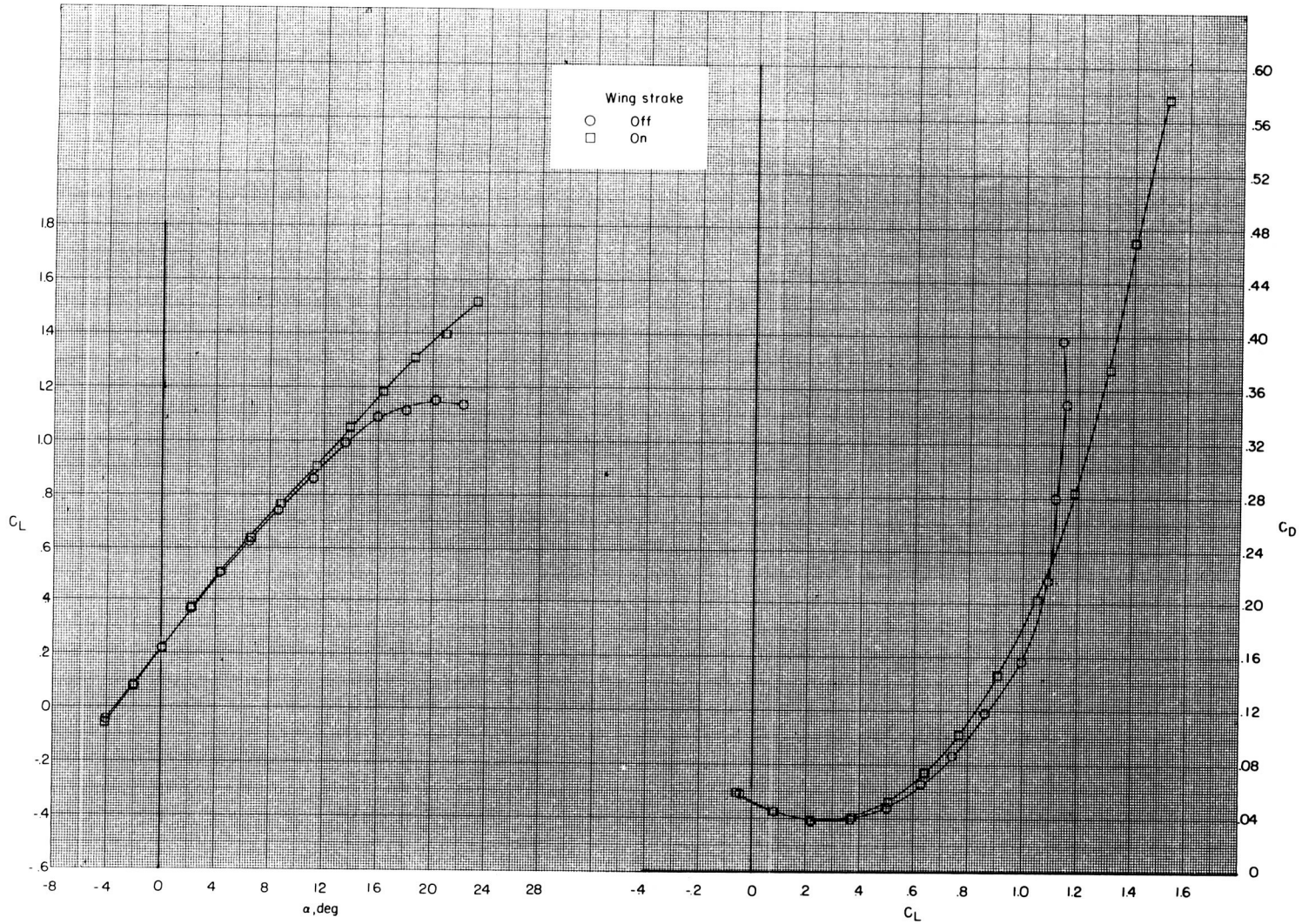

(c) M = 0.60.

Figure 10.- Continued.

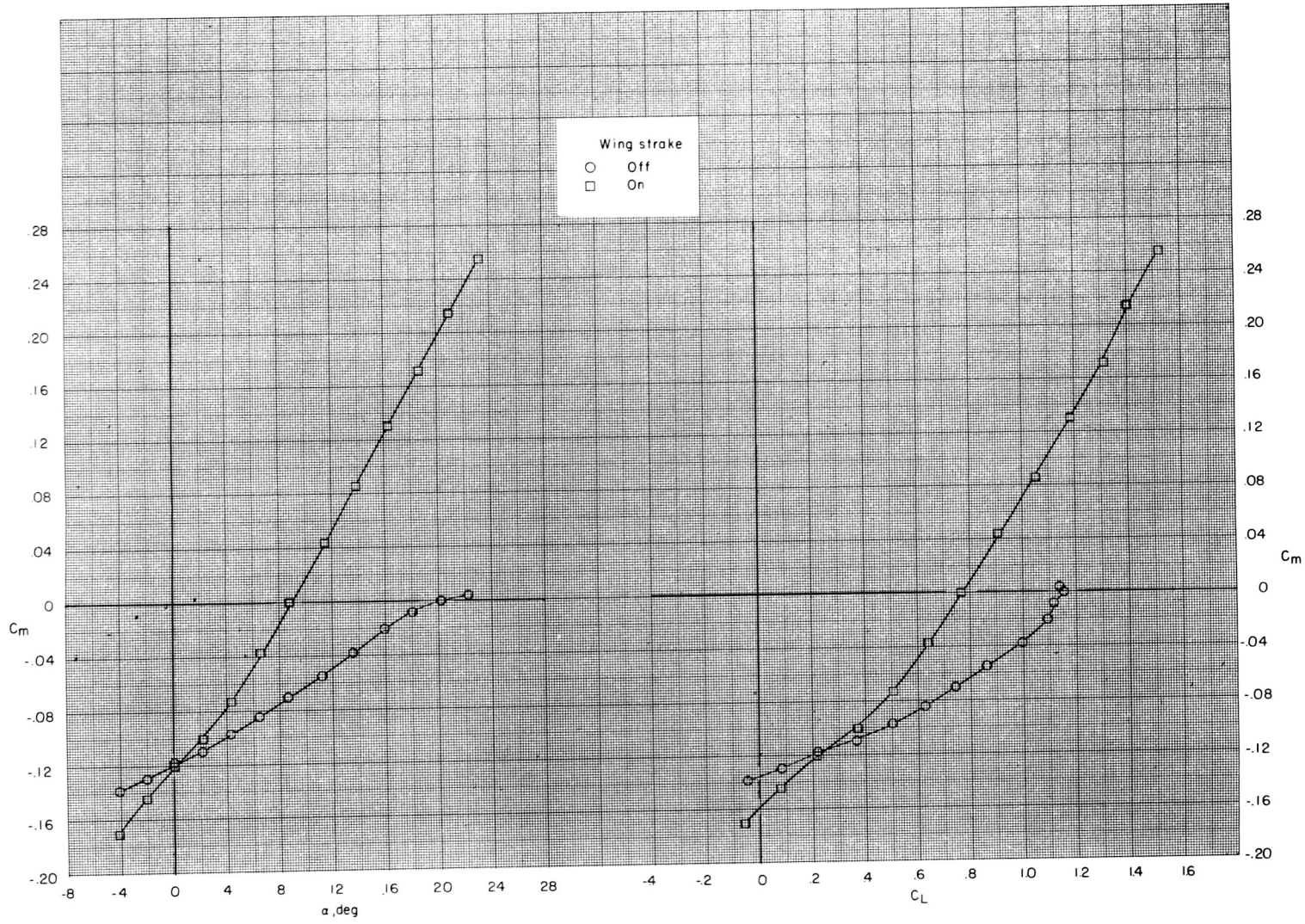

(c) Concluded.

Figure 10.- Continued.

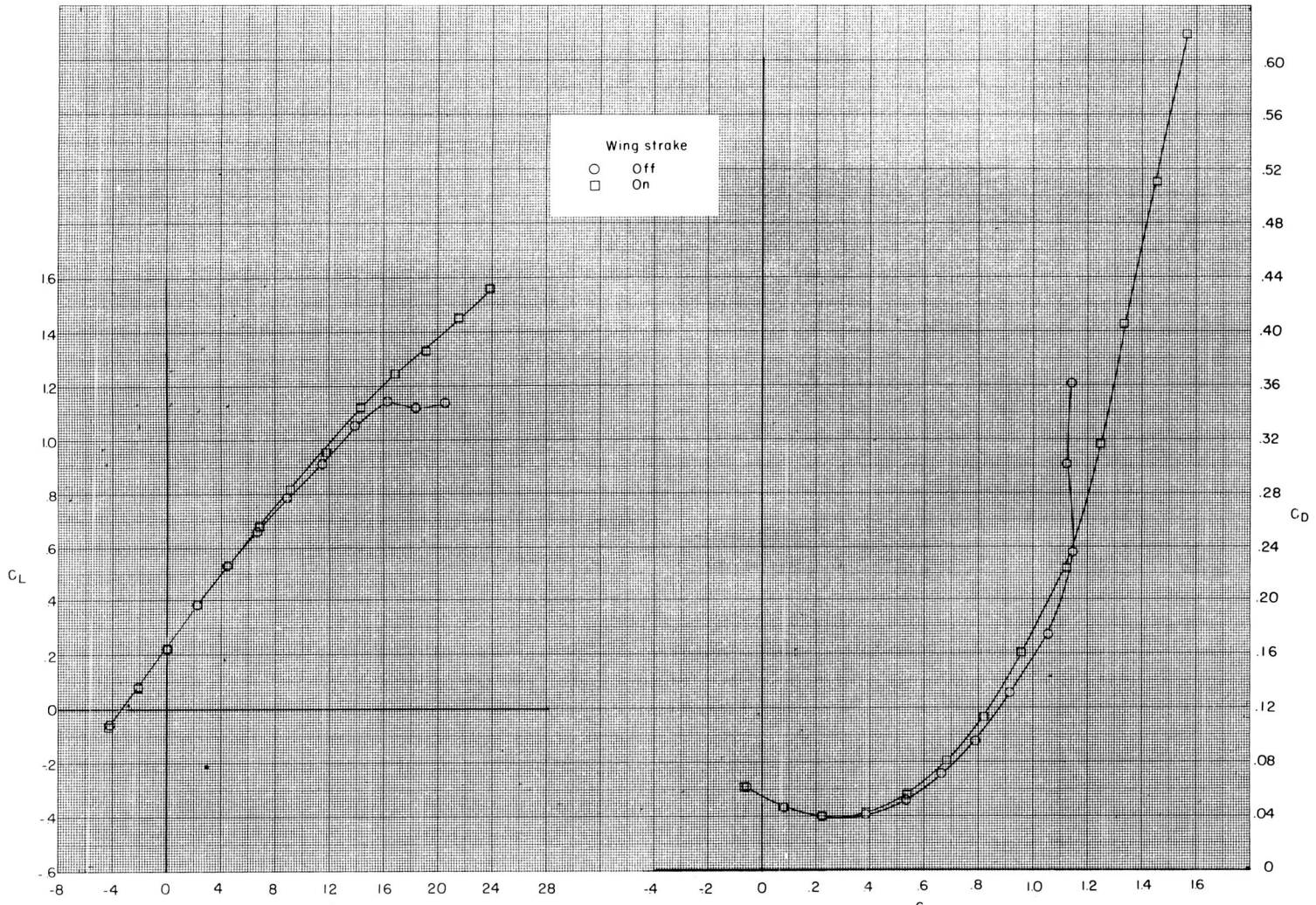

(d) M = 0.70.

Figure 10.- Continued.

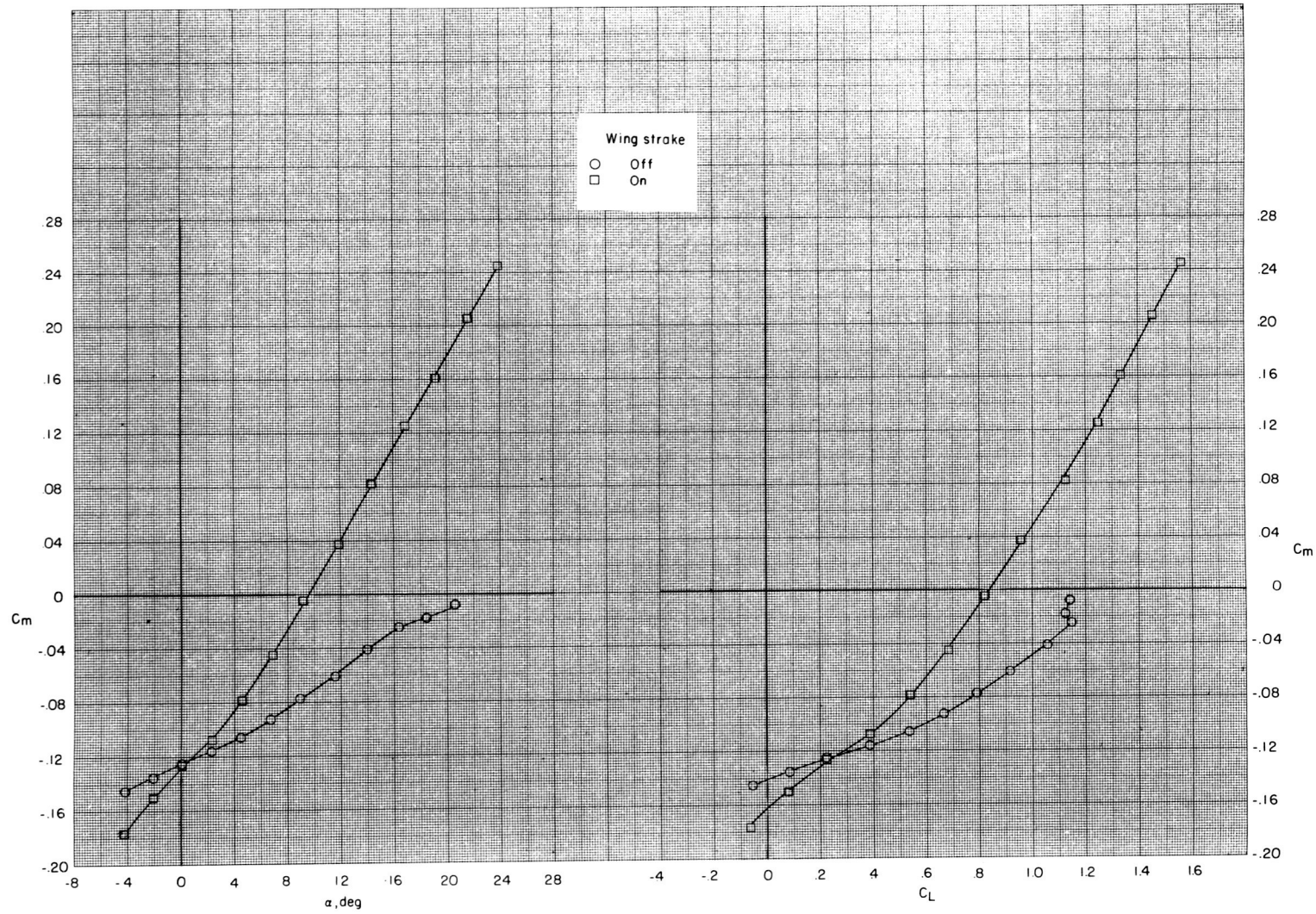

(d) Concluded.

Figure 10.- Concluded.

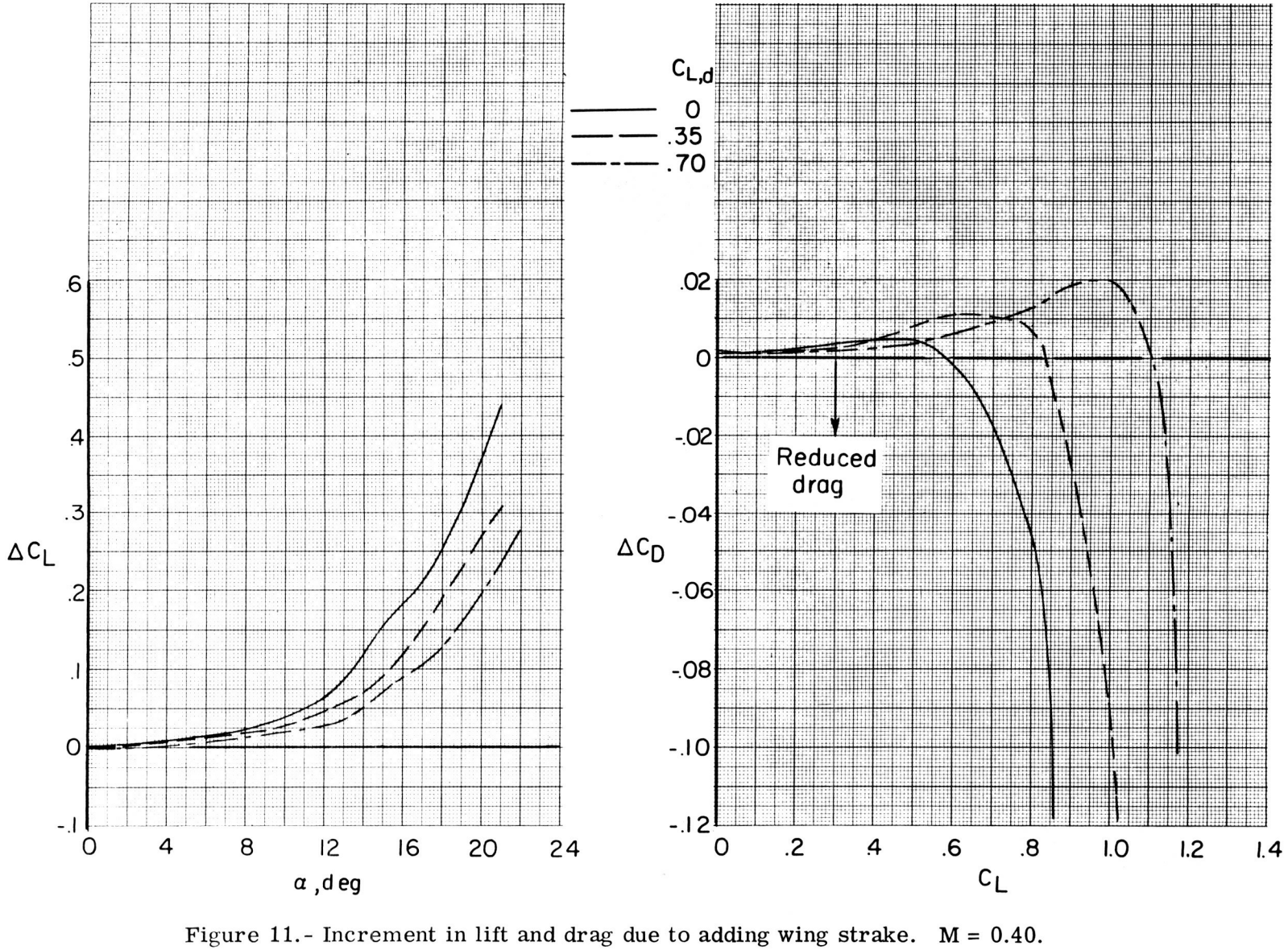

Figure 11.- Increment in lift and drag due to adding wing strake. M = 0.40.

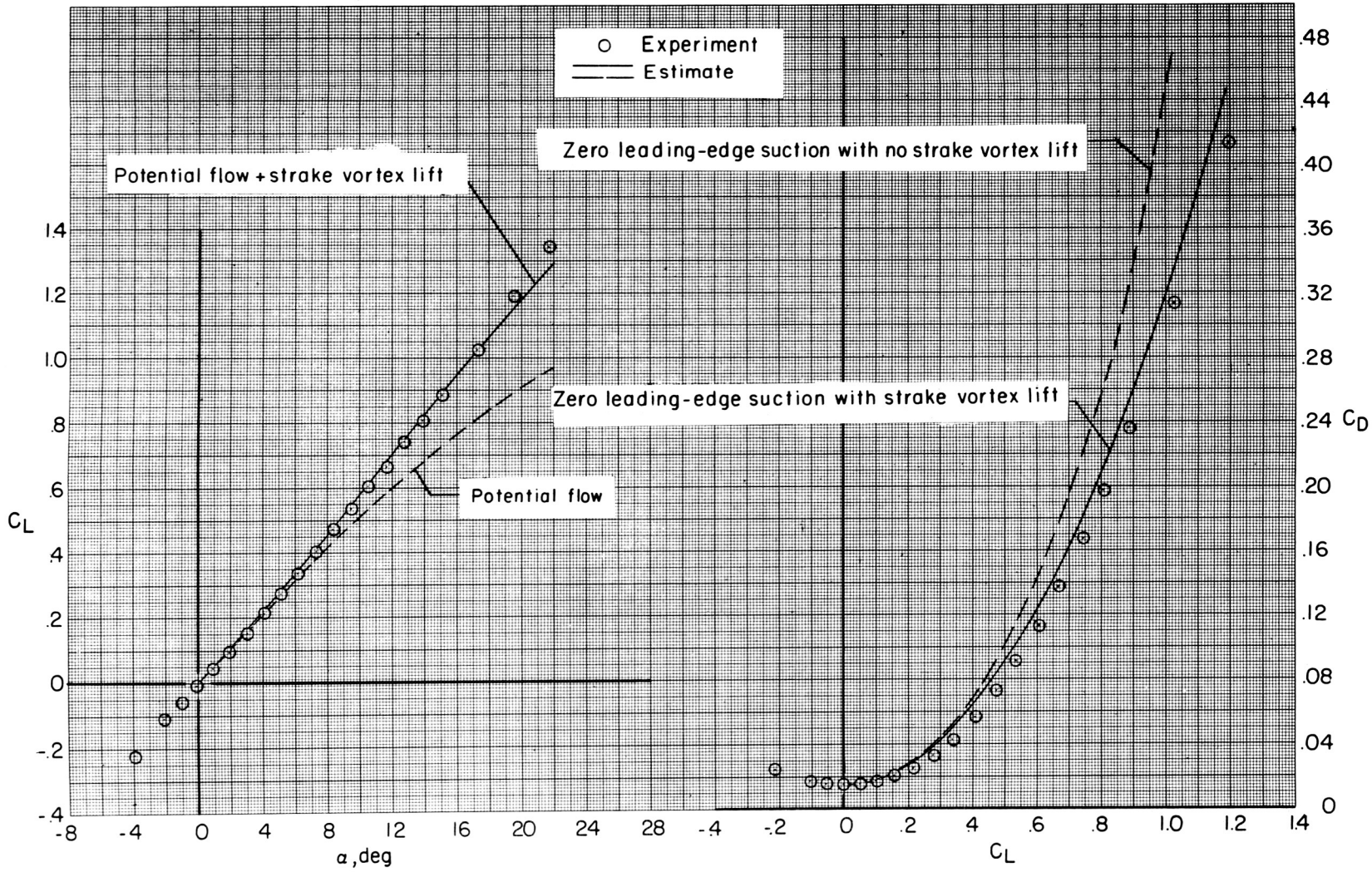

Figure 12.- Comparison of experimental and estimated lift and drag for model with strake. $C_{L,d} = 0$.